



National Library
of Canada

Bibliothèque nationale
du Canada

Canadian Theses Service

Services des thèses canadiennes

Ottawa, Canada
K1A 0N4

CANADIAN THESES

THÈSES CANADIENNES

NOTICE

The quality of this microfiche is heavily dependent upon the quality of the original thesis submitted for microfilming. Every effort has been made to ensure the highest quality of reproduction possible.

If pages are missing, contact the university which granted the degree.

Some pages may have indistinct print especially if the original pages were typed with a poor typewriter ribbon or if the university sent us an inferior photocopy.

Previously copyrighted materials (journal articles, published tests, etc.) are not filmed.

Reproduction in full or in part of this film is governed by the Canadian Copyright Act, R.S.C. 1970, c. C-30. Please read the authorization forms which accompany this thesis.

**THIS DISSERTATION
HAS BEEN MICROFILMED
EXACTLY AS RECEIVED**

AVIS

La qualité de cette microfiche dépend grandement de la qualité de la thèse soumise au microfilmage. Nous avons tout fait pour assurer une qualité supérieure de reproduction.

S'il manque des pages, veuillez communiquer avec l'université qui a conféré le grade.

La qualité d'impression de certaines pages peut laisser à désirer, surtout si les pages originales ont été dactylographiées à l'aide d'un ruban usé ou si l'université nous a fait parvenir une photocopie de qualité inférieure.

Les documents qui font déjà l'objet d'un droit d'auteur (articles de revue, examens publiés, etc.) ne sont pas microfilmés.

La reproduction, même partielle, de ce microfilm est soumise à la Loi canadienne sur le droit d'auteur, SRC 1970, c. C-30. Veuillez prendre connaissance des formules d'autorisation qui accompagnent cette thèse.

**LA THÈSE A ÉTÉ
MICROFILMÉE TELLE QUE
NOUS L'AVONS REÇUE**



National Library of Canada

Bibliothèque nationale du Canada

0-315-24916-1

Canadian Theses Division

Division des thèses canadiennes

Ottawa, Canada
K1A 0N4

PERMISSION TO MICROFILM — AUTORISATION DE MICROFILMER

• Please print or type — Écrire en lettres moulées ou dactylographier

Full Name of Author — Nom complet de l'auteur

BRUCE GEORGE VEIDT

Date of Birth — Date de naissance

JAN. 03, 1959

Country of Birth — Lieu de naissance

CANADA

Permanent Address — Résidence fixe

c/o GEORGE VEIDT
BOX 12
GRIMSHAW, ALBERTA
T0H 1W0

Title of Thesis — Titre de la thèse

A 408 MHz SYNTHESIS RADIO TELESCOPE

University — Université

UNIVERSITY OF ALBERTA, EDMONTON, ALBERTA

Degree for which thesis was presented — Grade pour lequel cette thèse fut présentée

MASTER OF SCIENCE, ELECTRICAL ENGINEERING

Year this degree conferred — Année d'obtention de ce grade

1984

Name of Supervisor — Nom du directeur de thèse

J.F. VANELDIK / T.L. LANDECKER

Permission is hereby granted to the NATIONAL LIBRARY OF CANADA to microfilm this thesis and to lend or sell copies of the film.

The author reserves other publication rights, and neither the thesis nor extensive extracts from it may be printed or otherwise reproduced without the author's written permission.

L'autorisation est, par la présente, accordée à la BIBLIOTHÈQUE NATIONALE DU CANADA de microfilmer cette thèse et de prêter ou de vendre des exemplaires du film.

L'auteur se réserve les autres droits de publication; ni la thèse ni de longs extraits de celle-ci ne doivent être imprimés ou autrement reproduits sans l'autorisation écrite de l'auteur.

Date

July 20, 1984

Signature

Bruce Veidt

THE UNIVERSITY OF ALBERTA

A 408 MHZ SYNTHESIS RADIO TELESCOPE

by



BRUCE VEIDT.

A THESIS

SUBMITTED TO THE FACULTY OF GRADUATE STUDIES AND RESEARCH
IN PARTIAL FULFILMENT OF THE REQUIREMENTS FOR THE DEGREE
OF MASTER OF SCIENCE

DEPARTMENT OF ELECTRICAL ENGINEERING

EDMONTON, ALBERTA

FALL, 1984

THE UNIVERSITY OF ALBERTA
FACULTY OF GRADUATE STUDIES AND RESEARCH

The undersigned certify that they have read, and recommend to the Faculty of Graduate Studies and Research, for acceptance, a thesis entitled "A 408 MHz SYNTHESIS RADIO TELESCOPE" submitted by Bruce George Veidt in partial fulfillment of the requirements for the degree of Master of Science.

J. Mandik
.....
Supervisor

T. Landecker
.....
Supervisor

M. B. L. D. D.
.....

P. F. F.
.....

D. Routledge
.....

ABSTRACT

The synthesis radio telescope at the Dominion Radio Astrophysical Observatory at Penticton, British Columbia has been modified to observe simultaneously with a second continuum channel. To accomplish this, the 1420 MHz feed horns were modified and new independent receivers were added to the telescope.

The new dual-frequency feed consists of a coaxial-cavity feed horn designed for 1420 MHz operation within which 408 MHz monopoles have been placed. These probes excite the horn as a cylindrical waveguide horn. The presence of these probes has a negligible effect on the 1420 MHz performance. The edge illumination of the parabolic reflector by this feed is ~ 10 dB. The combination of the feed and reflector has the following performance: 5.3° half-power beamwidth; 60% aperture efficiency; 30K spillover; 52K zenith temperature excluding the galactic contribution.

A highly phase stable receiver has been developed that corrects for the signal path length uncertainties from the receiver mixers to the intermediate frequency outputs. The stability of the receiver is at least seven times better than earlier receiver systems that only stabilized the local oscillator phase. The receiver uses GaAsFET low noise amplifiers with an effective noise temperature of 50K, which results in a typical system temperature of 104K excluding the galactic contribution.

The design of this system is described in this thesis. Detailed analysis of the phase locked loop in the local oscillator is also included. System tests are described and preliminary results from the first complete survey at 408 MHz (the HB3 supernova remnant) are shown.

ACKNOWLEDGMENTS

This thesis would not have been possible without the help and encouragement of many people. I must thank my supervisors, Tom Landecker, Dave Routledge, and Fred Vaneldik for their encouragement and for sharing their knowledge of radio astronomy instrumentation with me. I must also thank John Galt and Lloyd Higgs (directors of the Dominion Radio Astrophysical Observatory) for allowing me to do my thesis work at the Observatory.

Everyone at the Observatory has helped me in one way or another. Two technicians, Ev Sheehan and Rod Stuart, assisted in the manufacture and installation of my designs. Peter Lawson and Ron Casorso also constructed pieces of electronic equipment. Harry Mielke machined components for this project. Geoff Croes and Carman Costain modified the telescope software to enable 408 MHz observations to be made. I had many useful conversations with Jim Caswell regarding the interpretation of the first observations made with the telescope. Cindy Furtado typed this thesis. Erika Rohner handled the paperwork for ordering parts. I am indebted to these people and their colleagues for making this thesis possible and for making my stay at the Observatory a very worthwhile and enjoyable experience.

My parents have always encouraged me throughout my studies and this is appreciated very much.

Financial support was received from the NRC and from NSERC grants to Drs. Routledge and Vaneldik.

The components used in the construction of this radio telescope receiver were purchased using funds donated to the Observatory by Grote Reber. I hope that he will consider the construction of this telescope to be a worthy use of his gift.

TABLE OF CONTENTS

Chapter	Page
1. THEORY AND JUSTIFICATION OF 408 MHz TELESCOPE	1
A. Introduction	1
B. Mechanisms of Radio Emission	1
C. Aperture Synthesis Theory	4
D. The DRAO Supersynthesis Telescope	11
E. Justification of 408 MHz Addition to Telescope	15
F. What Has Been Done	17
G. What Had To Be Done	18
2. 408 MHz ANTENNA	20
A. Introduction	20
1. Requirements for a "Good" Reflector Antenna Feed	20
2. Antenna Test Range Measurements	23
B. 1420 MHz Reception	25
C. Modification for 408 MHz Radiating Structure	30
D. Combining Network	44
E. Frequency Independence Measurements	52
F. Performance on Dish	54
1. Dish Radiation Patterns	55
2. Aperture Efficiency	59
3. Spillover	59
G. Conclusion	61

3.	408 MHz RECEIVER	62
	A. The General Problem	62
	B. Receiver Front Ends	68
	C. Automatic Gain Control	75
	D. The Local Oscillator System and Phase Stability	78
	1. Need for Phase Stability	78
	2. Sources of Phase Instability	81
	3. Phase Stabilization Techniques Used With Other Telescopes	84
	4. Theory of 408 MHz Local Oscillator	86
	5. Design of 408 MHz Local Oscillator	95
	Sources of Error	95
	Voltage Controlled Oscillator	100
	Phase Detector and Loop Filter	103
	Synthesizers	109
	204 MHz Source	112
	Phase Shifter	113
	RF/DC Combining Network	117
	RF Combining Network	121
	Coaxial Line	127
	Phase Locked Loop Design	130
	Filter Specification	146
	Packaging of the System	149
	6. System Tests	151
4.	ASTRONOMICAL OBSERVATIONS	167
	A. Introduction	167
	B. Repeatability	167

C. Long-term Phase Stability	169
D. Solar Interference	172
E. Man-made Interference	174
F. Cross Talk	175
G. Telescope Dynamic Range; Observations of 3C295	176
H. Telescope Sensitivity: Maps of the 5C2 Region	182
I. A Complete Survey: HB3 Supernova Remnant	187

LIST OF FIGURES

Figure	Page
1.1 Typical Continuum Radio Spectra	5
1.2 Basic Interferometer	8
2.1 Dimensions of SST Feed	26
2.2 Theoretical Patterns and Aperture Distributions	27
2.3 Radiation Patterns of Feed Horn at 1420 MHz	31
2.4 408 MHz Probe Dimensions	36
2.5 Return Loss of One Probe	38
2.6 Radiation Patterns of Feed Horn at 408 MHz	42
2.7 Antenna Combining Network	46
2.8 Return Loss of Entire Feed System	53
2.9 408 MHz Primary Radiation Pattern	58
3.1 Block Diagram of a Radio Astronomy Receiver	63
3.2 GaAsFET Low Noise Amplifier	70
3.3 Automatic Gain Control	77
3.4 Elementary Phase Stabilized Local Oscillator	88
3.5 Phase/Frequency Scheme of Local Oscillator System	93
3.6 Local Oscillator for One Receiver	94
3.7 Voltage Controlled Oscillator	102
3.8 PLL Phase Detector and Loop Filter	106
3.9 PLL Lock Detector	107
3.10 15 MHz Digital Synthesizer	111
3.11 Phase Shifter Switch Driver	115

3.12	Phase Shifter PIN Diode Switch	117
3.13	RF/DC Combining Network	119
3.14	RF/DC Combining Network Return Loss vs. Frequency	119
3.15	RF Combining Network	123
3.16	Input Impedances of the Components Connected to the RF Combining Network	125
3.17	High Frequency Combining Network Characteristics	128
3.18	Phase Locked Loop Simplified for Control System Analysis	132
3.19	Root Locus Plots	141
3.20	Response of PLL to Noise on VCO Control Voltage	142
3.21	Calculated Closed Loop Response of PLL	145
3.22	Local Oscillator Spectrum	158
3.23	LO Phase Error vs. Line Length	161
3.24	Long-term Phase Stability	164
4.1	Repeatability of Visibility Measurements	168
4.2	Calibration Phase vs. Time at 408 MHz	170
4.3	Calibration Phase vs. Time at 1420 MHz	171
4.4	An Example of Solar Interference	173
4.5	Map of 3C295 Region Before CLEANing	177
4.6	Map of 3C295 Region After CLEANing	179
4.7	Map of Region 2.65° North of 3C295	181
4.8	Identified Sources in 5C2 Region	183
4.9	CLEANed 5C2 Map with Residuals Added	184
4.10	Second 5C2 Map with Residuals	185
4.11	408 MHz Map of HB3 and Environs	190
4.12	408 MHz Map of HB3 SNR	191

LIST OF PHOTOGRAPHIC PLATES

Plate	Page
1.1 DRAO Synthesis Telescope	13-14
2.1 Dual Frequency Feed Horn	40-41
2.2 Focus Box	56-57
3.1 Exterior View of LO Remote Chassis	152-153
3.2 Interior View of LO Remote Chassis	154

CHAPTER 1: BACKGROUND THEORY AND JUSTIFICATION OF 408 MHZ TELESCOPE

A. Introduction

For the length of man's collective memory, the sky with its luminous bodies has been viewed with wonder. It is this curiosity that has motivated the construction of new and better telescopes. The system to be described has added a second observing frequency to an existing radio telescope and will allow astronomers to learn more about the structure, composition, and dynamics of objects within and outside the galaxy.

In this chapter the fundamental theory explaining the sources of radio emissions as well as the basic principles of aperture synthesis imaging with radio telescopes will be put forth. The Supersynthesis Telescope (SST) at the Dominion Radio Astrophysical Observatory (DRAO) will also be described and the need for an additional observing band of frequencies on this telescope will be justified. Further chapters will describe the design and testing of the dual-frequency feeds and highly stable receivers, and will also present the first observations made with the telescope.

B. Mechanisms of Radio Emission

After Hertz's verification of Maxwell's Equations, a number of experimenters attempted without success to measure the electromagnetic radiation at radio frequencies from celestial objects such as the sun.

The first detection of radio waves of extraterrestrial origin occurred when Jansky (1933) identified the galactic center as the origin of 20 MHz radio noise. Reber (1940, 1944) made the first radio maps of the sky at 160 MHz and 480 MHz. Other workers have built instruments, some of which followed up these early efforts with greater sensitivity and resolution; others explored the sky at different wavelengths, including infrared, ultraviolet, and x-ray radiation.

Radio emissions can be divided into two classes: broadband or continuum radiation and narrow band radiation from spectral lines. Radio spectral lines (both emission and absorption), like optical lines, are the result of quantum changes in energy levels of atoms or molecules and are related to frequency by Planck's constant. The best known radio spectral line is the neutral hydrogen line at 1420 MHz ($\lambda=21\text{cm}$) which is the result of a small energy change when the spin direction of the electron changes (van de Hulst 1945). Line observations are useful because the emission is highly monochromatic at a well known frequency which enables velocity measurements to be made using the Doppler effect. The neutral hydrogen in our own galaxy as well as others has been mapped using this technique (Oort, Kerr and Westerhout 1958).

Continuum radiation is the result of other mechanisms which can be deduced from the shape of the spectrum. One type of continuum is "free-free" emission (Heney and Keenan 1940) which is a thermal

process that involves the interaction of free electrons and protons in clouds of ionized hydrogen (termed HII regions). At low frequencies the spectrum rises with an intensity proportional to f^2 until a turnover frequency is reached where the intensity becomes proportional to f^{-1} . At low frequencies the cloud is called "optically thick" because of its high attenuation of radio waves propagating through it. As a result, the radiation from this region is primarily due to thermal radiation from the cloud itself. The Rayleigh-Jeans approximation to blackbody radiation can be used to describe the emission, and from this relation comes the f^2 dependence. As the frequency increases, the cloud becomes largely transparent or "optically thin" and radiation is due to either background sources or the cloud itself. At these frequencies the attenuation is a function of frequency ($f^{-2.1}$) and the net effect is an almost exact cancellation of the frequency dependence causing the spectrum to flatten. This type of emission can be seen around regions of recent star formation. After the star condenses out of a cloud of cold neutral hydrogen, it ionizes the surrounding hydrogen with ultraviolet radiation. The Orion nebula, a well-known optical object, is an example of an HII region.

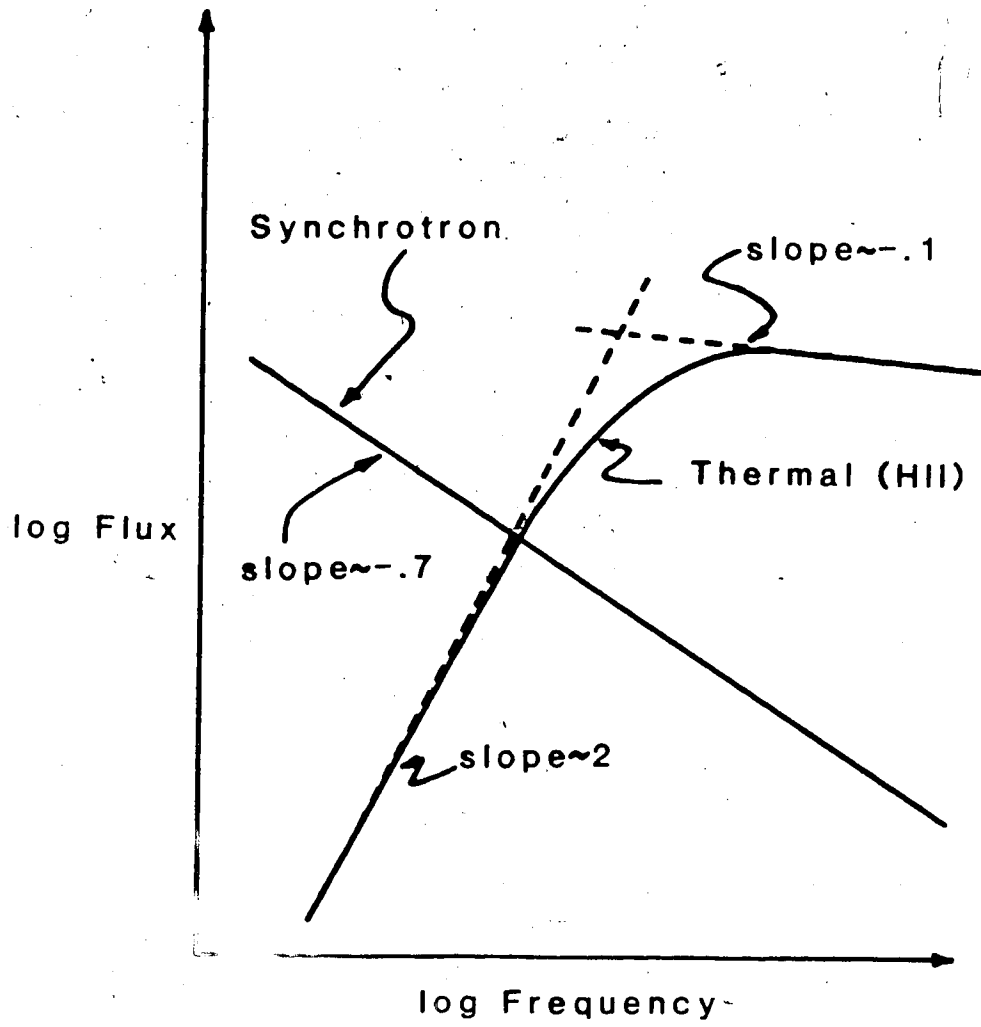
A second continuum radiation mechanism is synchrotron emission, which is the result of relativistic electrons (a component of cosmic rays) moving through interstellar magnetic fields (Kiepenheuer 1950). As they are decelerated, electromagnetic radiation is emitted. Objects such as supernova remnant shells, radio galaxies, and jets from radio

galaxies can be observed via synchrotron emission, and have spectra with intensity proportional to $f^{-\alpha}$ where α is between 0.3 and 0.9 typically.

It should now be apparent that observations at a number of frequencies help to identify the type of object and to understand the physical processes occurring within the object. Figure 1.1 shows the two types of continuum spectra described above.

C. Aperture Synthesis Theory

Telescopes with large apertures are desirable for two reasons: the greater the collecting area, the greater the telescope's sensitivity; and apertures of larger extent have narrower reception beams and allow the fine structure of sources to be studied. Unfortunately, the size of radio telescopes is limited by the strength of the materials that they are made of. The 100m Effelsberg dish in West Germany is the largest fully steerable filled-aperture radio telescope in the world. The Arecibo antenna in Puerto Rico at 300m is larger, but it can only point near the zenith. Fortunately, the technique of aperture synthesis can be used to produce the same results that telescopes kilometres or even thousands of kilometres in diameter would obtain if they existed (Blythe 1957).



Typical Continuum Radio Spectra

Figure 1.1

An intuitive argument can be used to show that this is possible. Consider first a large reflector antenna. Waves reflecting off the surface meet at the focus and reinforce or cancel depending on the sources' locations relative to the telescope pointing. Now suppose that the sources have constant brightness so that the amplitude and phase of waves reflecting off different parts of the dish do not change with time. Because of this time invariance, only a small part of the reflecting surface need be present at any one time, as long as the amplitude and phase of the wavefront are preserved in the recording process at the focus. Over a period of time, the small piece of reflecting material is moved to all parts of the dish surface and as all the wavefronts are recorded, an image is formed at the focal plane. The phase information can be preserved if two reflecting panels are used, one of which is stationary and provides a phase reference while the other is moved. This minimum set of apparatus is known as an interferometer.

Much more rigorous explanations of aperture synthesis exist (Fomalont 1973, Fomalont and Wright 1974). The explanation to be given here is similar to that used by Dewdney (1978). This theory will help establish some of the specifications of the receiver system.

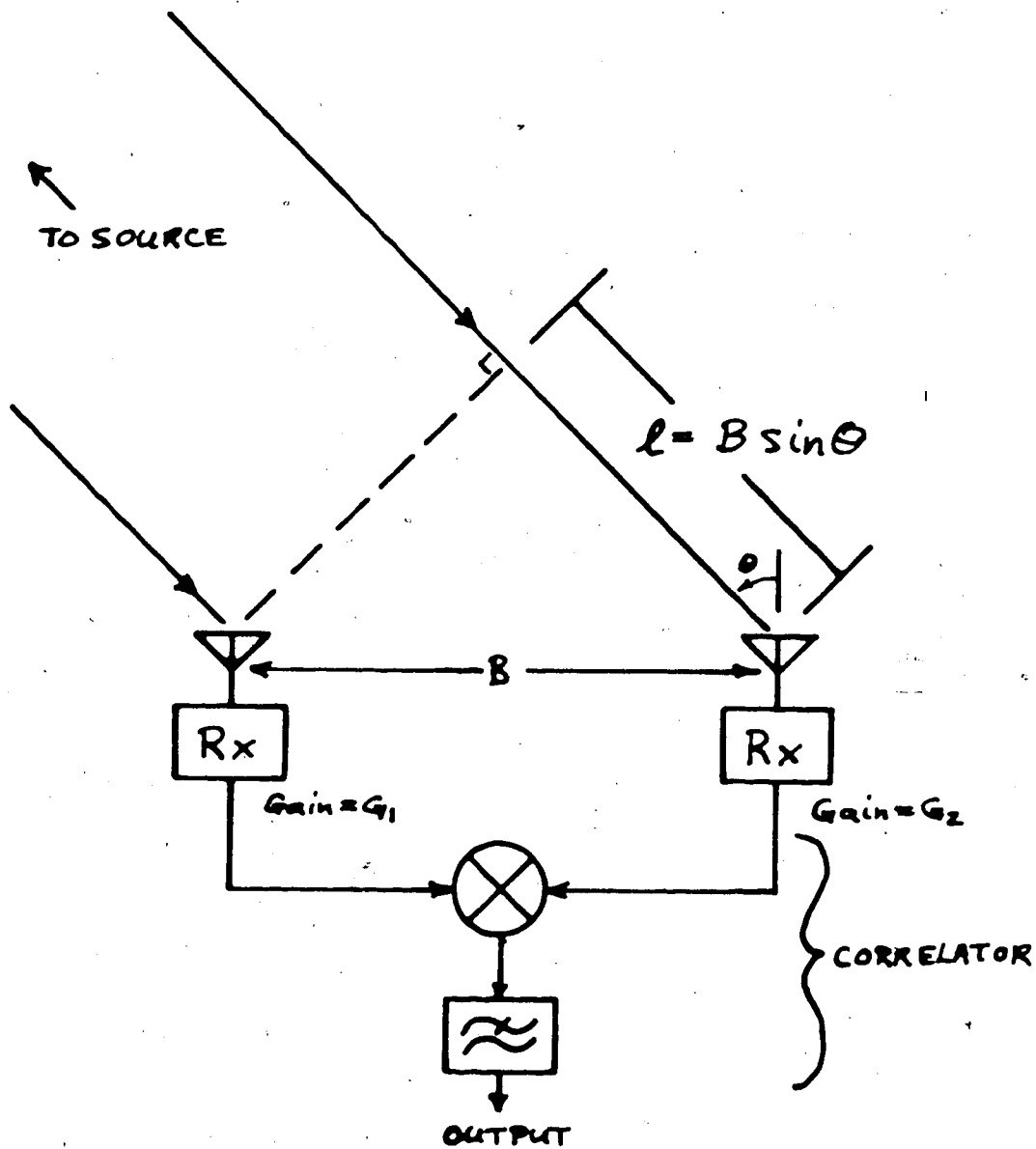
A basic interferometer (see Fig. 1.2) consists of two antennas separated by a baseline B connected to cables that carry the output of the receivers to a central point, where the signals are

crosscorrelated. The correlator multiplies the two signals together and a lowpass filter extracts the difference product, which contains information on the amplitude of the signals intercepted by the antennas, and the phase difference between the two signals which arises as a result of the array-source geometry.

Now suppose the response of the interferometer is mapped by moving a monochromatic test source on the celestial sphere while noting the correlator output. (The "celestial sphere" has earth at its centre, and is arbitrarily large so that effects of the interferometer's displacement from the centre of the earth is negligible.) Of course the output will be modified by the antenna beams and by shadowing by the earth, but for the moment these two effects will be ignored. The array is rotationally symmetric about the line joining the two antennas, so if the source moves within a plane perpendicular to the line B, the correlator output does not change. However, moving the source within a plane which contains the line B changes the source-array geometry and the correlator output changes. Figure 1.2 shows that the correlator output for a source of unity intensity is:

$$C(\theta) = Ge^{j2\pi(B/\lambda)\sin\theta}$$

where G is the gain of the interferometer and λ is the observing wavelength.



$$\text{Phase} = 2\pi \frac{l}{\lambda} = 2\pi \left(\frac{B}{\lambda}\right) \sin \theta$$

$$\text{Gain (Power)} = \sqrt{G_1} \sqrt{G_2} = G$$

Interferometer Response:

$$C(\theta) = G e^{j2\pi \left(\frac{B}{\lambda}\right) \sin \theta}$$

Basic Interferometer

Figure 1.2

Now suppose that the baseline is aligned in an east-west direction. As the earth rotates, this two-dimensional interferometer pattern sweeps across the sky and the correlator real channel output has quasi-sinusoidal fluctuations, or fringes. The output of the correlator at any one time is the complex sum of the source intensities after they have been multiplied by the interferometer response. At other times the fringe pattern on the sky is aligned in different directions with respect to the sources, and the correlator outputs (called visibilities) can be different. Since the interferometer response is known, with enough independent visibility measurements (obtained by observing at different times and with different baselines), the brightness distribution in the sky can be deduced and a map drawn.

For practical reasons, the visibility measurements occur in discrete intervals of time, the baseline is adjusted in fixed step sizes, and the map of the sky is drawn with a regular grid of pixels. Thus these numbers can be placed in matrices. The measured visibilities and the gridded sky brightness can be related as follows:

$$\mathbf{V} = \mathbf{eI}$$

\mathbf{V} is a matrix containing the visibilities, \mathbf{I} has the sky brightness distribution and \mathbf{e} contains the computed interferometer responses for the source pixel locations in \mathbf{I} and for the measurement position in \mathbf{V} . Inversion of the above equation will produce a map of the sky. If the angle θ is small, the interferometer

response can be approximated by

$$Ge^{j2\pi(B/\lambda)\theta}$$

and when this is substituted into the above equation, the brightness distribution is related by the discrete Fourier transform to the visibility measurements. This is the usual case, and for this reason visibilities are often called the Fourier components of the map.

There are only two points on the celestial sphere where the angle θ is small for all rotation angles of the earth - the two celestial poles. So far the fringes on the sky have been fixed with respect to the earth, but they can be rotated at will by injecting the proper phase into the receivers. Thus, the fringes can be stopped at any point in the sky. Since the position angle of the array baseline viewed from the source rotates through 360° in 24 hours, the fringes also rotate about this point in the sky. In other words, the interferometer's "north pole" or phase centre can be moved to any point on the sky through "fringe stopping". When the field of view is restricted by the antennas' primary patterns, the fringe rate is small since observed sources are near the phase centre. The slower fringes are advantageous because this allows the use of integrators with longer time constants. The restricted field of view means that there are fewer sources in the map (than the entire sky) and hence fewer visibility measurements are needed to unambiguously define the source positions and strengths.

Another modification to the basic interferometer is necessary to

allow it to measure any point on the sky: the time delay from the source through the antennas and receivers must be equalized. This is necessary because the signals from the sky are broadband noise, and decorrelation occurs if the two signals are offset in time in the correlator.

This technique is known as earth rotation aperture synthesis or supersynthesis (Ryle 1962) since the earth's rotation is used to scan the area to be mapped with the interferometer response pattern. Almost all modern radio telescope arrays utilize this method.

It is apparent that to obtain an accurate map, the matrix e must be well known. Instrumental gain and phase can be determined with calibration observations of isolated point sources for which the visibilities are easy to calculate. During regular observations between calibrations the stability of the system must be depended upon.

D. The DRAO Supersynthesis Telescope

The DRAO SST is located in a semi-arid mountain valley near Penticton, British Columbia. The primary observing frequency is nominally 1420 MHz and the instrument can map a $2^\circ \times 2^\circ$ region of the sky with 1 arcminute resolution. The telescope can simultaneously produce continuum radiation maps and spectral line maps of neutral hydrogen emission (absorption). Details of the instrument and performance

statistics are given by Roger et al (1973) and Purton (1983). The telescope is shown in Plate 1. This thesis describes the modification of the telescope to produce continuum maps at 408 MHz simultaneously with its 1420 MHz outputs.

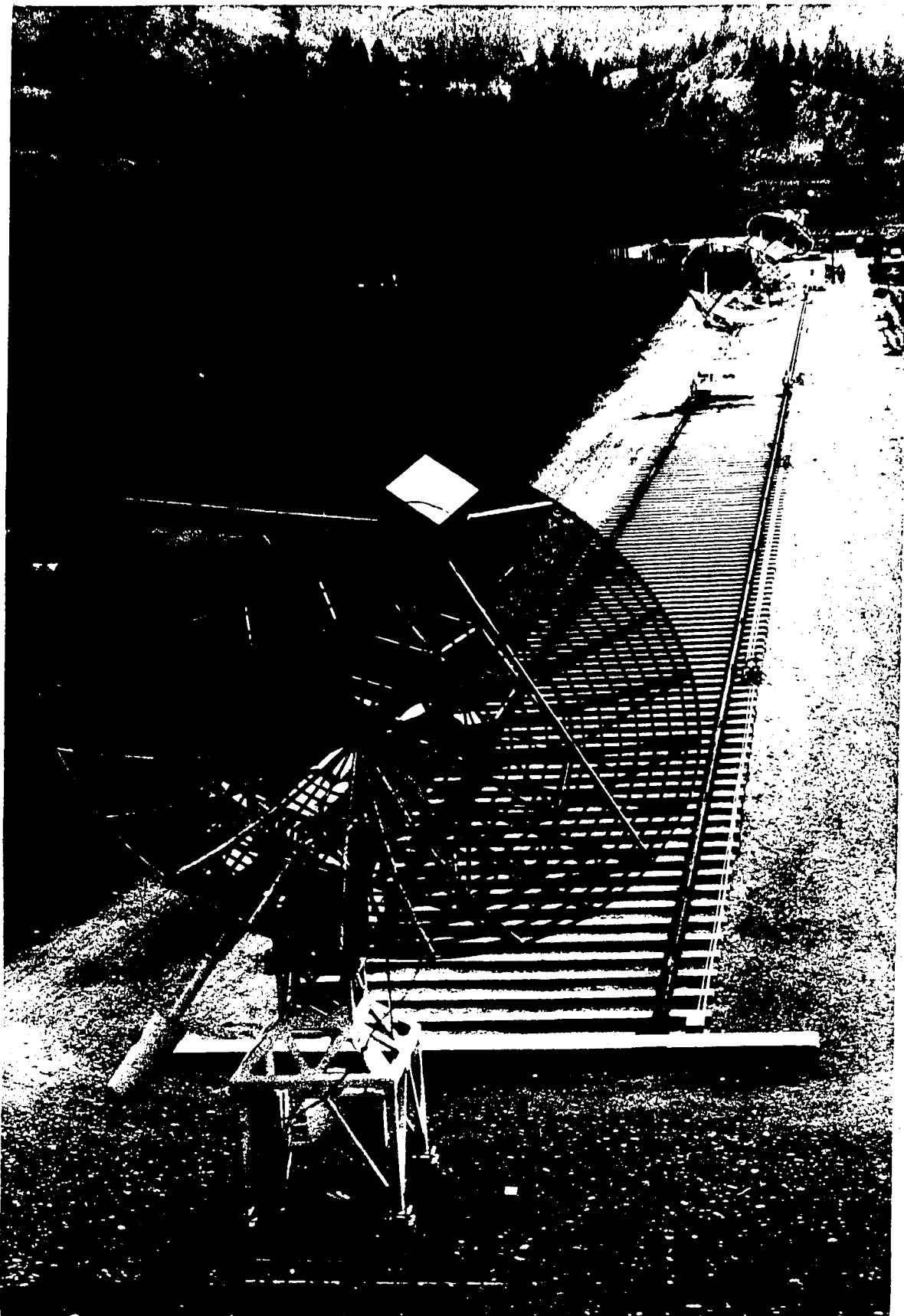
The antenna array consists of four 9 metre paraboloidal reflector antennas on an east-west baseline 600 metres long. Two antennas are fixed at each end of the baseline, while the other two can be moved along a precision railway track. The track is 300 metres long and runs from the centre to the west end of the array. Seventy observing locations are marked along the track, so for a complete survey with both movable dishes, thirty-five 12-hour observing periods are required.

The individual antennas are prime focus reflector antennas. The receiver front end electronics (low noise amplifier, mixer, local oscillator, and intermediate frequency amplifier) are located immediately behind the feed in a temperature controlled enclosure called the focus box. The dishes are on equatorial mounts, and the positioning is automatically controlled by the observing computer.

Coaxial cables run from the dishes to the centre of the telescope where they enter the Synthesis TeTelescope building. The cable is buried in the sandy ground along most of its length. Three cables are

Plate 1.

This is a view of the DRAO Synthesis Telescope as seen from the west. All four dishes, along with the precision railway track are visible.



supplied to each dish: one for the 1420 MHz local oscillator; one for the 1420 MHz intermediate frequency; and a spare.

This telescope has a wide field of view and moderate resolution when compared with other instruments. This makes the instrument very well suited for mapping objects that are within our own galaxy, some of which have an angular extent larger than the field of view of other telescopes. Although astronomers are continually striving for greater resolution, the moderate resolution of this telescope does have an important advantage. As the resolution is increased, the sensitivity to extended structures (as opposed to point sources) decreases since less power is captured by the narrower beam from broad structures, but the same power is received from point sources. Thus the wide field of view coupled with the moderate resolution and good sensitivity to extended sources makes the telescope very useful in the study of supernova remnants and HII regions. Examples of such observations are given by Landecker et al (1982) and Dewdney and Roger (1982). The telescope has also been used to observe extragalactic objects such as the Andromeda Galaxy and clusters of galaxies.

E. Justification of 408 MHz Addition to Telescope

A second continuum observing frequency on the SST will be valuable for a number of reasons. The spectral indices of sources will be determined rapidly by comparing the two maps produced. Previously,

observations from other observatories had to be used if they were available. With the second observing channel, these measurements will be made simultaneously and with a telescope whose instrumental parameters are very accurately known, and similar in nature to those of the primary frequency.

Another reason for adding a low frequency channel to the SST is that the intensity of synchrotron emissions increases with decreasing frequency so that the telescope will become better able to observe broad, diffuse structures. This capability is also aided by the improvement in sensitivity due to the broader synthesized beam of the second frequency system.

The frequency of 408 MHz was selected for a number of reasons. It is a protected frequency band (406.1 to 410 MHz) with radio astronomy as the primary user (ITU 1982). Other radio astronomy bands exist at 327 MHz and 610 MHz, but 408 MHz was chosen for these reasons:

- a compact 327 MHz feed would be more difficult to build than a 408 MHz feed;
- the resolution would be lower at 327 MHz
- the ionosphere is $(408/327)^2 \approx 1\frac{1}{2}$ times worse at 327 than 408 MHz;
- a full-sky radio survey at 408 MHz exists (Haslam et al. 1981, 1982) which can be used to supply the very short interferometer spacings that cannot be measured.

A low frequency observing capability is also considered to be desirable by other observatories. At the Very Large Array in the United States and at the Westerbork Synthesis Radio Telescope in the Netherlands 327 MHz feeds and receivers are being developed (Napier 1982, de Bruyn and van der Hulst, 1983) and low frequency channels will be included on the Australia Telescope.

F. What Has Been Done

Prior to the commencement of this thesis project some work had been done by myself and other workers. The general specifications for the second channel were written by Landecker (1980). The new 1420 MHz feeds had been developed by myself and others, although the 408 MHz feed structure had not been developed yet. As I began my work, Lo was completing a unique digital correlator (Lo 1982).

The microprocessor-based digital correlator or Digital Signal Processor (DSP) does a number of processes in software which were previously done with hardware: the correlator imaginary channel is obtained from the real channel by a scheme of interpolation; fringe derotation phase is injected after the correlator, and not before as with most previous synthesis telescopes; and the fine delay compensation is done by interpolating between measurements at discrete delay steps. As well, coarse delay compensation is performed with digital gates so that the large analog cable delay lines as used with the 1420 MHz system are not required for the 408 MHz system.

Traditional complex correlators actually consist of two correlators: one that provides the real part of the correlation coefficient; and another correlator that is identical except for a 90° phase shift applied to one input so that the output is rotated 90° and the imaginary part of the correlation coefficient appears. This phase shift can also be applied after correlation to obtain the imaginary channel. In the microprocessor implementation, 16 correlations separated by delay steps are obtained with digital hardware, and the real channel component at zero delay is obtained through interpolation. The imaginary channel is then obtained with a different interpolation function. This complex pair of numbers is then phase shifted (to stop the fringes) to obtain the correct visibilities. These visibilities are calculated for all interferometer pairs and are transmitted to the host computer which accumulates and writes the numbers onto hard disk.

The DSP also controls the local oscillator phase in 90° steps, so that the interferometer can be calibrated, and for phase switching of the receiver in regular observations.

G. What Had To Be Done

Receivers and feeds for each of the four dishes were required with the following specifications:

- nominal centre frequency of 408 MHz;
- 4 MHz bandwidth;
- high degree of gain and phase stability;
- intermediate frequency and local oscillator to share the same cable running from the dish to the synthesis telescope building;
- local oscillator phase controllable in 90° steps;
- 408 MHz feed structure that does not degrade 1420 MHz operation;
- antennas that combine maximum efficiency with minimum spillover.

The next two chapters will explain how these general specifications were met, and the last chapter will describe observations that demonstrate the performance of the telescope.

CHAPTER 2: 408 MHZ ANTENNA

A. Introduction

The feed horns for the dishes of the SST have been replaced with new feeds that not only improve the primary observing frequency (1420 MHz) performance, but also allow the dishes to receive 408 MHz radiation simultaneously. This new design originated with a single frequency coaxial feed horn for 1420 MHz that had a higher aperture efficiency with lower spillover noise than the old rectangular horn. Adding the structures necessary for 408 MHz reception did not degrade the primary frequency feed quality. The following antenna parameters were measured at the new frequency: aperture efficiency of 60%; antenna temperature at the zenith of 73K, and half-power beamwidth of 5.3°. This section will outline the design and testing of this new feed, emphasizing the 408 MHz aspects.

1. Requirements for a "Good" Reflector Antenna Feed

An ideal antenna would receive radiation from only one direction and reject completely radiation from all other directions. This can only be approximated in practice. For a prime focus reflector antenna the closeness to ideality depends upon two components - the reflector (its diameter and surface accuracy being crucial) and the characteristics of the feed antenna. Since for this project the reflecting surfaces were in existence, the only way to modify the

radiation characteristics of the antennas was to change the feed antennas.

From the transmitting point of view, the feeding antenna should illuminate the reflecting surface and nowhere else. Power radiated elsewhere is wasted power - it is not focused by the parabolic surface towards the desired direction. This is called spillover.

The reflector should be illuminated as uniformly as possible. If less than the full reflecting surface is illuminated, the width of the radiating aperture is smaller, and from the Fourier transform relation (Bracewell 1965), the width of the radiation pattern is greater than necessary. This means that the power is radiated over a larger solid angle, and the power radiated in the desired direction is reduced.

Both of these ideas can be looked at from a receiving point of view. If a reflector antenna suffers from spillover, then the feed antenna receives not only radiation off the reflecting surface from the desired direction, but also from beyond the edge of the dish. This radiation from beyond the dish edge can come from other celestial sources or it can be thermal radiation from the ground. Both of these, especially the latter, increase the noise level of the receiver, degrading its sensitivity.

The concept of aperture efficiency has been introduced from the transmitting viewpoint. If a receiving feed antenna receives power from only a small part of the reflecting surface, its efficiency is smaller than it could be because it is not receiving all the power intercepted by the reflector. In practice, only exceptional reflector antennas have an aperture efficiency greater than 50 or 60%.

A number of other characteristics are desirable:

- the radiation pattern should be circularly symmetric (ie. beamwidth in E plane and H plane should be identical);
- the level of the sidelobes should be low;
- the polarization response should be predictable.

Given a reflector that is circularly symmetric and has an accurate surface, these factors are almost entirely determined by the feed.

It is obvious that the feed parameters needed for these different antenna characteristics can be conflicting. For example, to keep the spillover low, the illumination at the dish edge should be low. This will probably result in lower antenna efficiency since to maximize the efficiency, the illumination should be high over the entire dish surface. Furthermore, with practical feeds, the amplitude response cannot drop to zero suddenly at the edge of the dish, so high edge illumination implies high spillover.

2. Antenna Test Range Measurements

The previous discussion has outlined the type of radiation pattern required for a good reflector antenna feed. The design procedure for the feed can be described as "cut and try". The radiation patterns were measured with an outdoor test range, and the antenna structure was changed to bring the antenna pattern closer to that desired.

Ideally, one would like to do pattern measurements in free space under these conditions: a source of radiation at infinity, the antenna under test capable of being positioned at will with respect to the test source, and nothing else. Of course a test range of this quality cannot be realized in practice, although an approximation was possible.

The wave from the source antenna must reach the test antenna via a direct path since reflected waves are received through a different part of the beam than that under study. To minimize reflections the test range was set up outdoors, away from structures containing metal such as buildings and fences. Reflections off the ground, test equipment and cables were minimized by covering these areas with mats made of carbon coated fibres. A simple experiment was used to test the quality of the test range: parallel dipole antennas were placed at the receiving and transmitting locations and were then rotated about the line connecting the two. Using the method of images, it can be shown that a horizontally polarized wave undergoes a 180° phase shift upon

reflection, while a vertically polarized wave does not. The vector sum of the direct and reflected rays may not be the same for the two orientations. Thus by changing the plane of polarization of the pair of antennas with respect to the ground, reflections will be indicated by variation in the received amplitude.

Another approximation that was made was to move the source antenna from infinity to a location closer to the earth. The minimum antenna separation is $2D^2/\lambda$ where D is the largest antenna dimension and λ is the wavelength (Hacker and Schrank 1982). At close spacings, one is in the near field (a region of stored rather than radiated energy) and sidelobes are difficult to resolve. With D equal to 0.6m and λ equal to 0.73m at 408 MHz, the minimum separation was about 1m. At 1420 MHz ($\lambda=0.21$ m), the minimum spacing was 3.4m. In practice 4 metres was used.

The antenna test range geometry was also important. The angle at which the reflected wave struck the ground was made as large as possible to minimize the reflection. With the test range used, the antennas were placed 2 metres above the ground so the angle of incidence was about 45°.

The quality of the test range was quite good at 1420 MHz. The difference between the main beam amplitudes in the two principal planes was less than 1 dB. The minor lobes were easily measured with dynamic

range of about 35 dB. This could only be done if spurious reflections were at a low level. The test range was not as good at 408 MHz, but it was still adequate. The difference in main beam amplitudes was 2-3 dB and the dynamic range was ~30 dB. The ground conductivity had a more significant effect at the lower frequency, and unfortunately, the summer when most of these measurements were taken was unusually wet.

B. 1420 MHz Reception

The design for this feed originated with Scheffer (1975). It is shown in Figure 2.1. The dimensions of the feed were optimized on an outdoor antenna test range for operation at 1420 MHz, and then the feed was modified for 408 MHz operation.

To uniformly illuminate a shallow reflector antenna (such as an optical Newtonian telescope which has a large f/D ratio), the feed pattern should be constant to the edge of the dish, then drop to zero, as shown in Fig. 2.2a. The Fourier transform of the radiation pattern is the feed's aperture field distribution, and for this particular case is

$$f(x) = c \frac{J_1(x)}{x},$$

where J_1 is the first order Bessel function and x is the radial displacement in units of wavelengths (Goodman 1968). Since the radiation pattern is circularly symmetric (assuming a circular reflector) so is the aperture distribution. A cut through this two

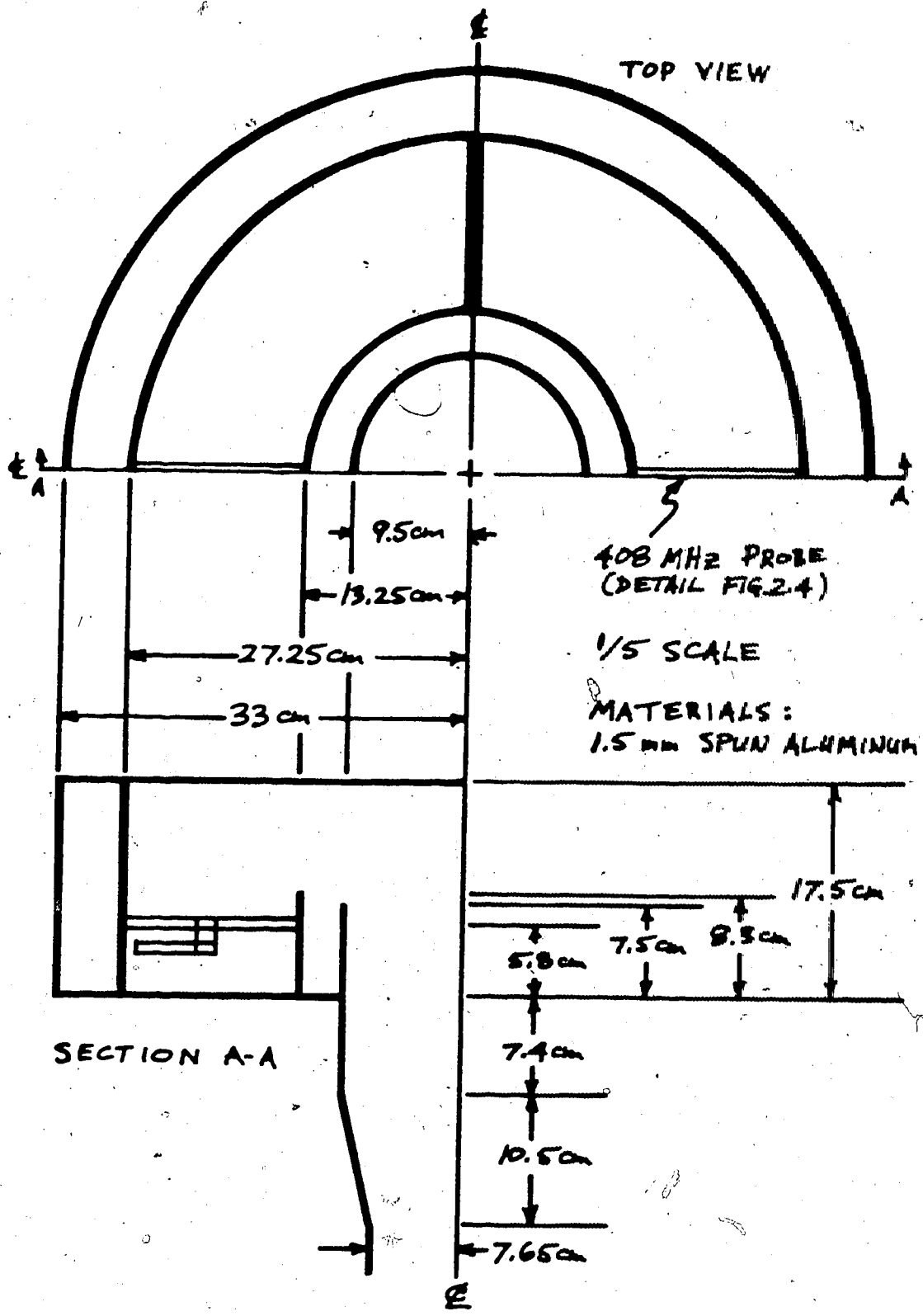


FIGURE 2-1 DIMENSIONS OF SST FEED

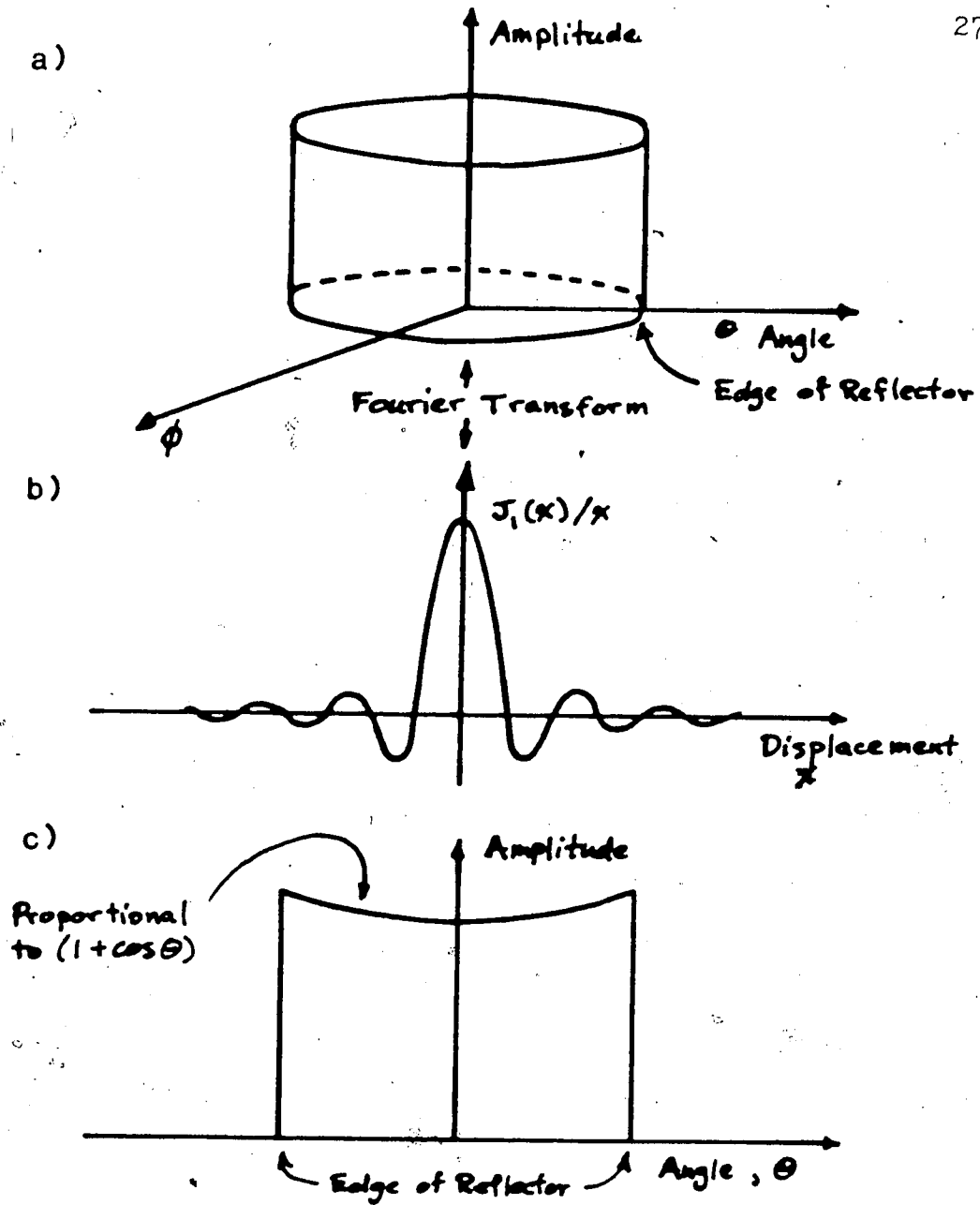


Fig. 2.2 (a) Feed radiation pattern to uniformly illuminate a shallow reflector. (b) Cut through aperture distribution needed to produce (a). (c) Cut through feed pattern for a deep parabolic reflector antenna with uniform illumination.

dimensional function is shown in Fig. 2.2b. This focal plane distribution is known to optical astronomers as Airy's rings.

There are a number of reasons why this aperture distribution is not optimum for radio telescopes. The most significant difference between optical telescopes and radio telescopes is the operating wavelength which makes radio telescopes very small when measured in terms of wavelength. Thus an optical telescope captures many of the higher order rings which often can't be used with a radio telescope without blocking a significant portion of the reflector area. Elimination of the higher order rings results in a smoothing of the sharp cutoff of the radiation pattern and the appearance of spillover lobes. Since the edge of the dish is no longer illuminated at full intensity, the illumination efficiency drops.

Another deviation from this ideal field distribution occurs because the distance from the feed to the reflecting surface is not constant; it is proportional to $1 + \cos\theta$ with θ being the off-axis angle. (This is also true with optical telescopes, but not to the same extent.) Thus the radiation pattern must also increase by the same factor to maintain the uniform aperture distribution, as illustrated in Fig. 2.2c. Minnett and Thomas (1968) have attacked this problem with much more rigor and have obtained equations describing the fields at the focal space of reflector antennas.

Although $J_1(x)/x$ is not a precise description of the fields at the focus, it is accurate enough to be a starting point for a design to be experimentally optimized. Koch (1973) and Scheffer (1975) describe feed horns developed in this way. Scheffer explains how this field distribution is obtained by superimposing several coaxial waveguide modes in the horn. A more simplistic explanation is that the main central lobe is supplied by the central circular waveguide, and the first ring lobe is generated in the large coaxial cavity, which is coupled to the waveguide across the narrow coaxial cavity. In practice, the proper coupling was achieved by varying the height of the two inner coaxial rings in a systematic fashion and measuring the feed horn pattern. The criteria for optimum adjustment were steep skirts, low edge illumination of the reflector, and a flat or concave main beam.

Later, in the modification of the feed for 408 MHz operation, another ring was placed around the outside of the horn to create an additional narrow coaxial cavity. The depth of this cavity is almost $\lambda/4$ at 408 MHz, so it presents a high impedance at the open end. This cavity is approximately $3\lambda/4$ deep at 1420 MHz, so it acts as a choke at that frequency as well. The total width is slightly less than the width of the focus box so the shadowing of the reflector was not changed.

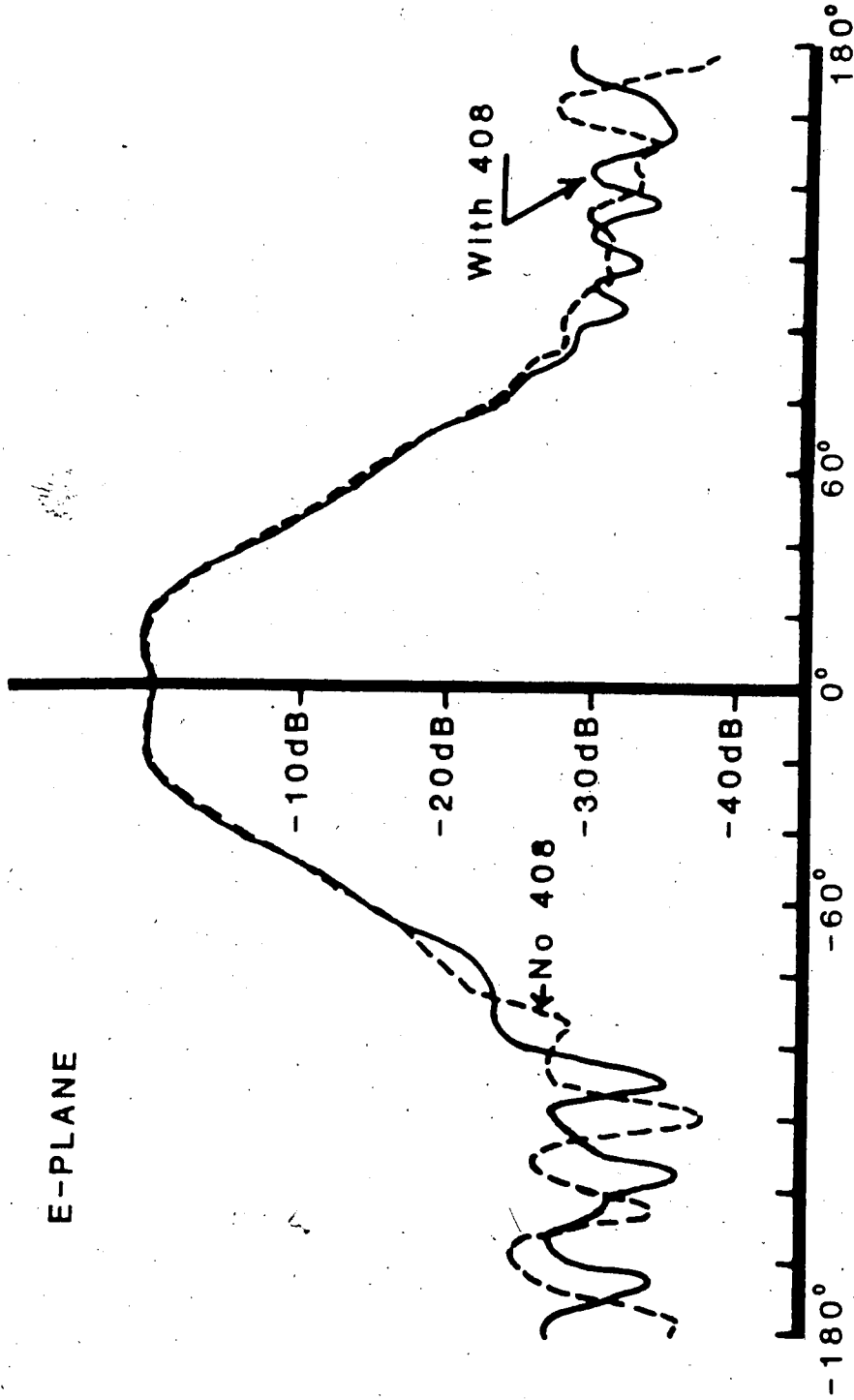
This feed has been configured to receive both hands of circular polarization. The coaxial transmission line to waveguide transition is at one end of the 14.95cm circular waveguide. This transition consists of two spatially orthogonal monopoles - one for each hand of circular polarization - in front of a short circuit plane at the end of the waveguide. The separation of the two senses of polarization is obtained with a quarter-wave-plate placed between the transition and the horn.

Antenna patterns at 1420 MHz are shown in Figure 2.3. The illumination at the edge of the dish ($\pm 60^\circ$) is -15 dB for the E plane and -17 dB for the H plane with respect to the on-axis (0°) intensity.

C. Modification for 408 MHz Radiating Structure

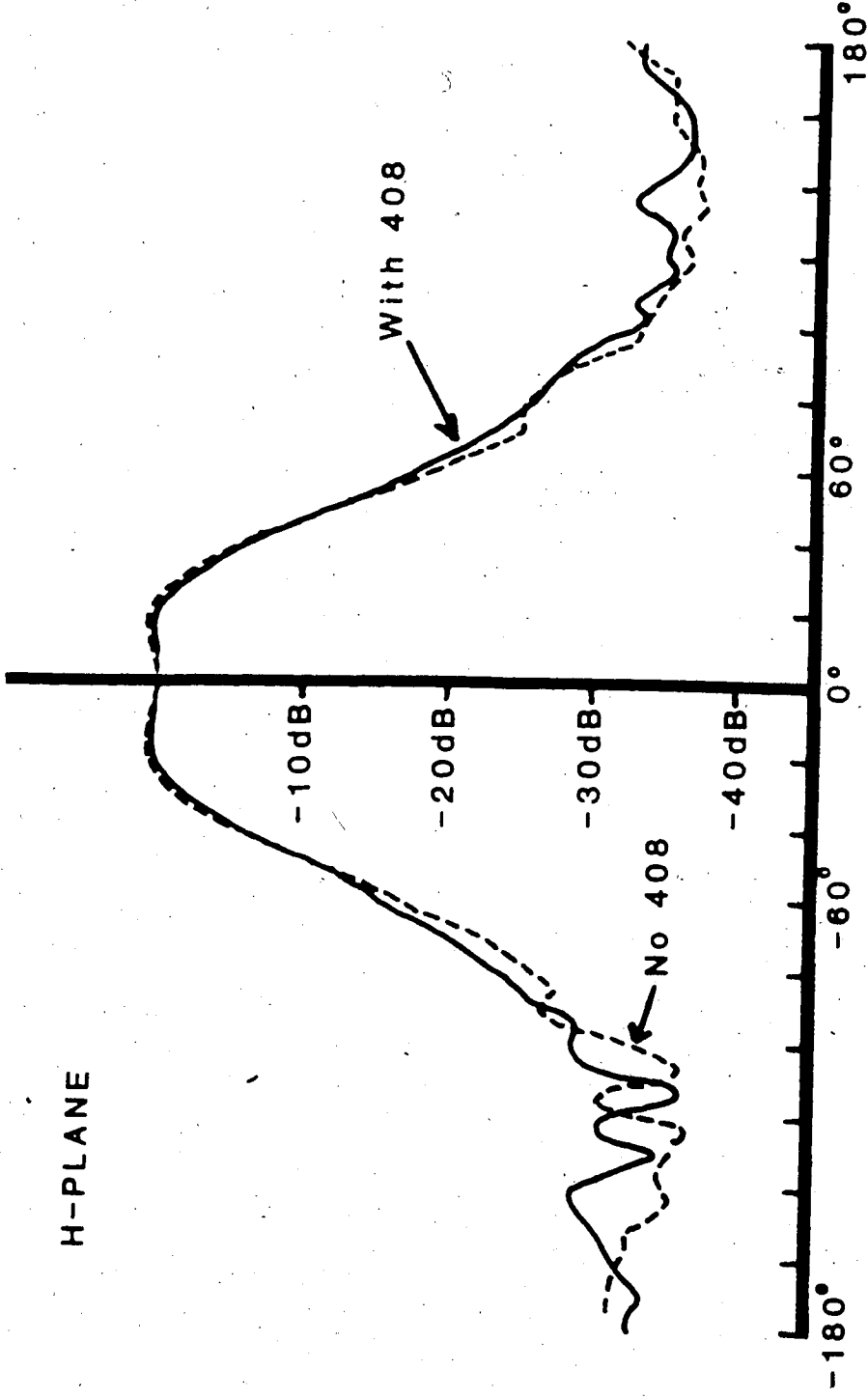
A number of different methods were tried in an attempt to add 408 MHz reception capability to the new 1420 MHz feed. Various designs were tested and discarded either because of distortion of the 1420 MHz radiation pattern, or because of inferior 408 MHz radiation patterns. Elementary array theory will show that an array of 408 MHz radiators whose first nulls lie at 60° or beyond must have the phase centres of the elements within the 1420 MHz horn. One such array that was tried consisted of four dipoles arranged in a square above a ground plane and is called a boxing ring antenna. Dipoles were placed in front of the feed to form this type of feed. This design was rejected because of

E-PLANE



Radiation Patterns of Feed Horn at 1420 MHz

Figure 2.3a



Radiation Patterns of Feed Horn at 1420 MHz

Figure 2.3b

large distortion to the 1420 MHz radiation pattern. Also, because the feed horn was a very crude approximation to a flat ground plane, the 408 MHz radiation pattern did not approach the predicted pattern. An array of cavity backed slots formed using the outer choke ring was also considered, but this idea was discarded because the maximum array element spacing was exceeded. The method finally chosen involves exciting the large cavity and using it as a waveguide horn. These modifications produced a feed with adequate performance at 408 MHz with negligible effect on the 1420 MHz operation.

From these experiments it was concluded that the method selected was the only practical method of adding a second frequency to the 1420 MHz feed horn.

The diameter of the large cavity is big enough to support TE_{11} modes at 408 MHz. Several other dimensions, however, are less than optimum. The cavity forms a coaxial waveguide over much of its length, and its length is short. These two factors together prevent an equal field from being established on the side of the horn opposite to the exciting structure. This would cause the beam to be steered off-centre. The solution to this was to use pairs of diametrically opposed radiators.

The radiators used are monopoles mounted one third the distance from the back of the cavity to the open end. Experiments with the feed

horn at 1420 MHz had shown that radial structures within the horn had no measurable effect on the radiation pattern. This was true even if a short circuit was connected across the large ring-cavity.

Measurements at 408 MHz were made with movable monopoles that could be moved towards either the front or the back of the horn. It was found that unless the monopole probes were very close to the open end or the back wall the radiation patterns were independent of the probe positions. What did depend upon the probe position was the input impedance which became smaller as the probe was placed nearer to the back wall. The position used was selected because it placed the probes well away from the mouth of the horn, which ensured that interaction with 1420 MHz was minimized, and also kept the radiation resistance large enough to be useful.

At this location the radiation resistance is low, typically 23Ω , and has a large capacitive reactance associated with it. The technique used to transform this radiation impedance to 50Ω is very similar to "gamma match" devices used on some Yagi antennas. The base of the monopole is connected to a ground plane (actually the wall of the large cavity), and the feed point is moved part way up the monopole. The radiator is fed through a parallel conductor running from near the base to the feed point, where it is joined to the monopole. The other end of the parallel conductor is attached to the centre of the coaxial transmission line through a small inductance chosen to cancel residual

capacitances. The construction details are shown in fig. 2.4. The theory of operation of the matching structure can be explained as follows (ARRL 1977). Three things occur simultaneously. First, the monopole is fed away from its base. This multiplies the base impedance by a factor $1/\cos^2\theta$ where θ is the distance from the base expressed in units of angle. Second, the parallel rods form an impedance transformer, just like the parallel conductors in a folded dipole. Since the conductors are equal diameter, the step-up ratio is 4:1. And finally, the parallel conductors form a balanced transmission line with a short circuit at the end. This places a shunt impedance at the output terminals. These three factors together determine the impedance.

The probe dimensions were obtained in the following manner. A prototype probe was constructed out of $\frac{1}{4}$ " copper tubing and brass shim stock with the total probe length and position of the bridge piece being variable. This was installed in the feed horn with three dummy probes made of single pieces of copper tubing. The impedance of the prototype was measured with a network analyzer, and the two variables were adjusted to move the real part of the impedance near the 50Ω circle. The imaginary part was measured at the center frequency and this determined the required series reactance to make the load resistive. An inductance was required, and was formed with a short piece of semi-rigid coaxial line with a short circuit at one end. The probes installed in the horn had fixed inductance and bridge pieces,

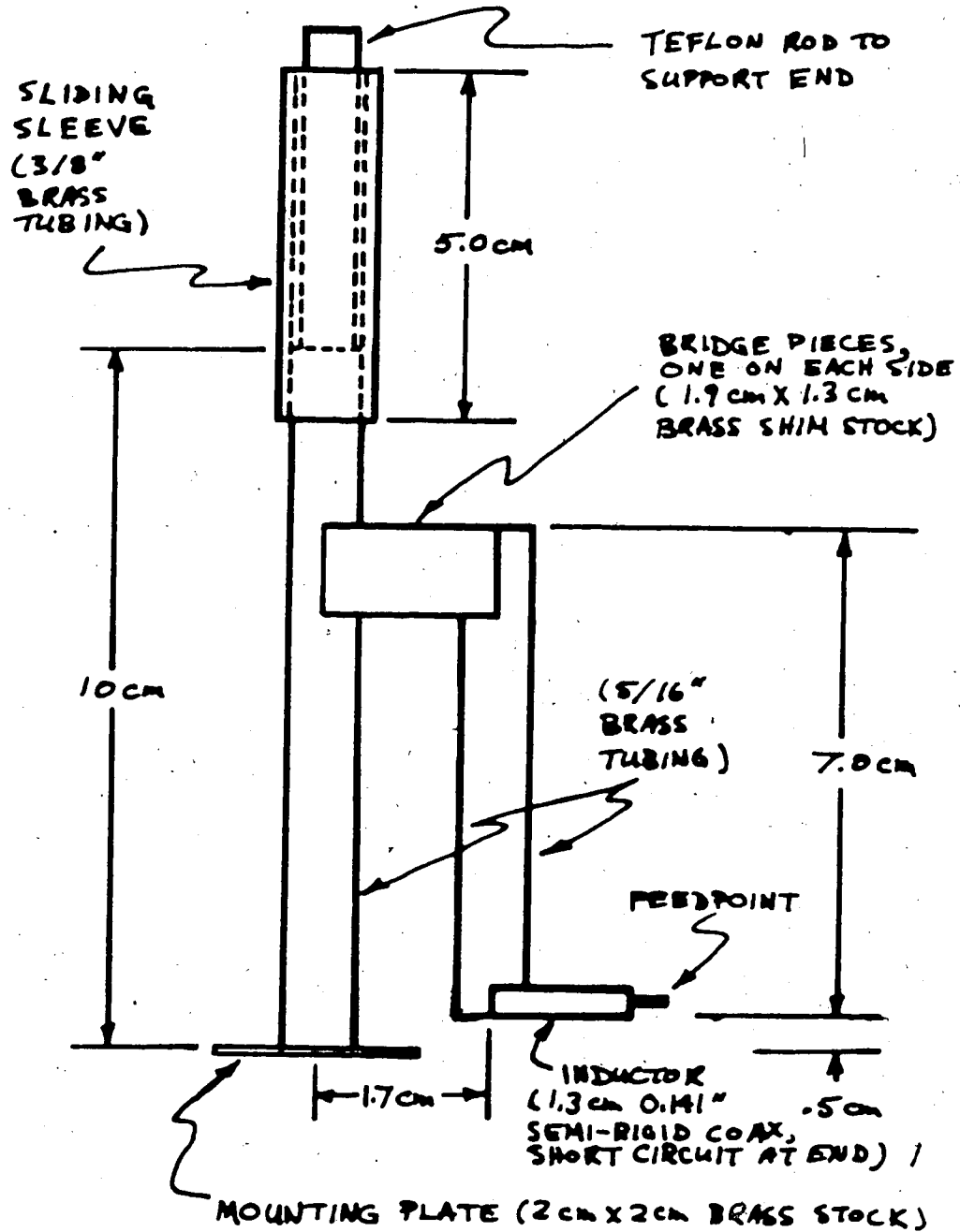


FIGURE 2.4 408 MHz PROBE DIMENSIONS (NOT TO SCALE)

and the probe length was left adjustable to compensate for component and structural variations.

The adjustment of one probe in the horn affected the adjustment of the others due to mutual coupling. Thus the probes all had to be tuned together, in an iterative sequential manner. The horn was pointed at the sky with the network analyzer connected to one probe and all the others terminated with 50Ω . This probe was adjusted for maximum and broadest return loss. An adjacent probe was then measured and adjusted. This process was continued around the horn until the probes had similar and maximum return losses. The adjustments were then fixed with solder.

Each probe was connected to a short length of semi-rigid coaxial cable that runs through the back wall of the feed to a type-N connector.

This telescope was being modified to observe broadband continuum radiation in a 4 MHz bandwidth centred on 408 MHz. In anticipation of man-made interference, the receiver was made tunable with the front-end filter spanning 403 to 413 MHz. The measured return loss of a probe over this range is at least 15 dB. Plots of return loss versus frequency are shown in fig. 2.5.

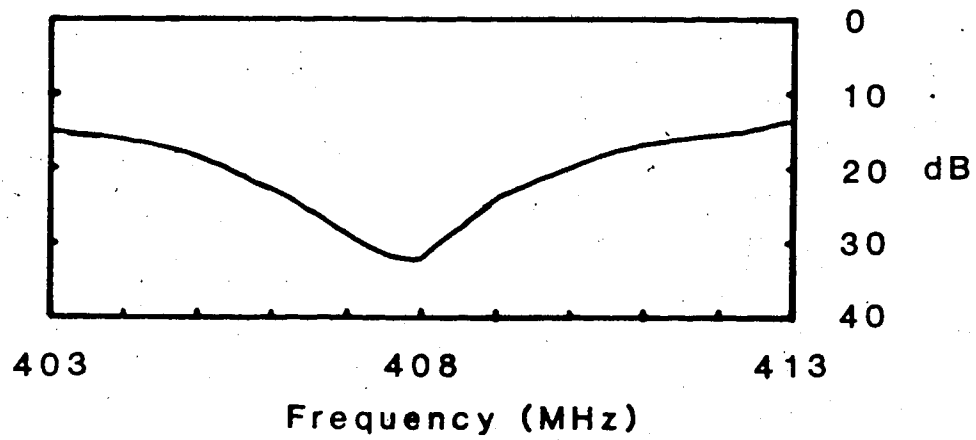
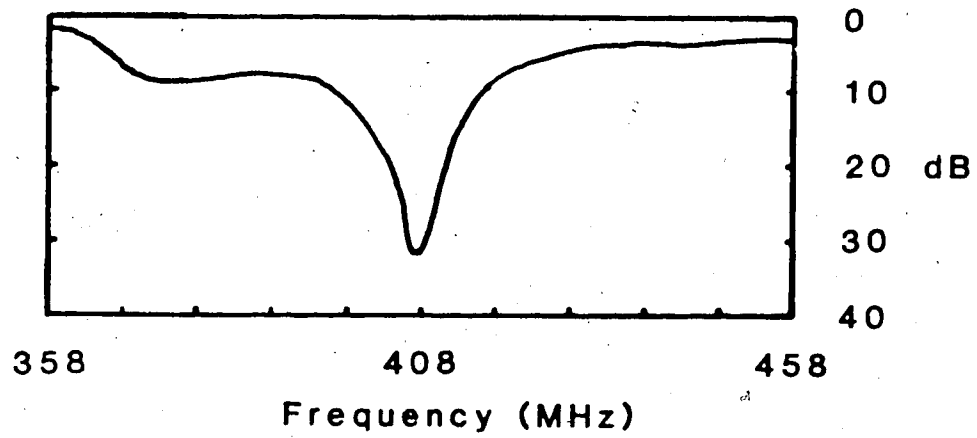


Figure 2.5 Return loss of one probe measured with the other probes tuned and terminated

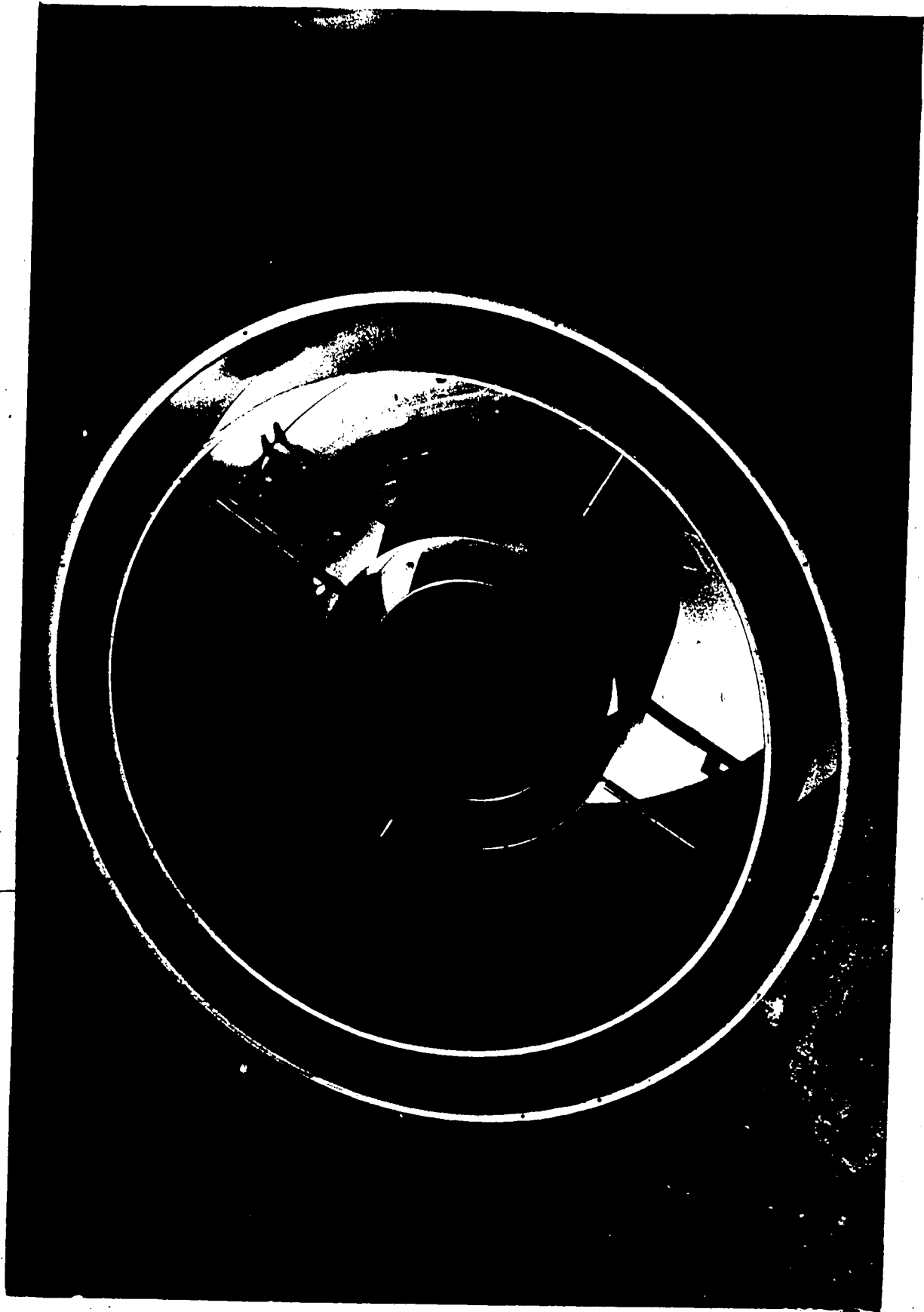
The complete dual frequency feed is illustrated in Plate 2.1. Typical radiation patterns at 408 MHz are shown in fig. 2.6. The shape of these radiation patterns is simple compared to the 1420 MHz patterns, since the horn is smaller at 408 MHz (in terms of wavelengths) than at 1420 MHz. The patterns show that the choke ring reduces the amplitude of the back lobe while leaving the main lobe virtually unaffected. This is because the high impedance of the choke reduces the currents flowing on the outside of the horn, while having little effect on the aperture (LaGrone and Roberts 1966). The patterns were also measured at 400 and 420 MHz. The variation in the main beam was less than $\frac{1}{2}$ dB. The back lobe varied less than 3 dB over this range.

The feed patterns are quite symmetrical and have edge illuminations ($\pm 60^\circ$) of -10 dB in both principal planes. The back lobes are less than -20 dB. It should be realized that in practice the radiation patterns near 180° will be modified by the focus box, and these measurements give an inaccurate description of the actual patterns at these angles.

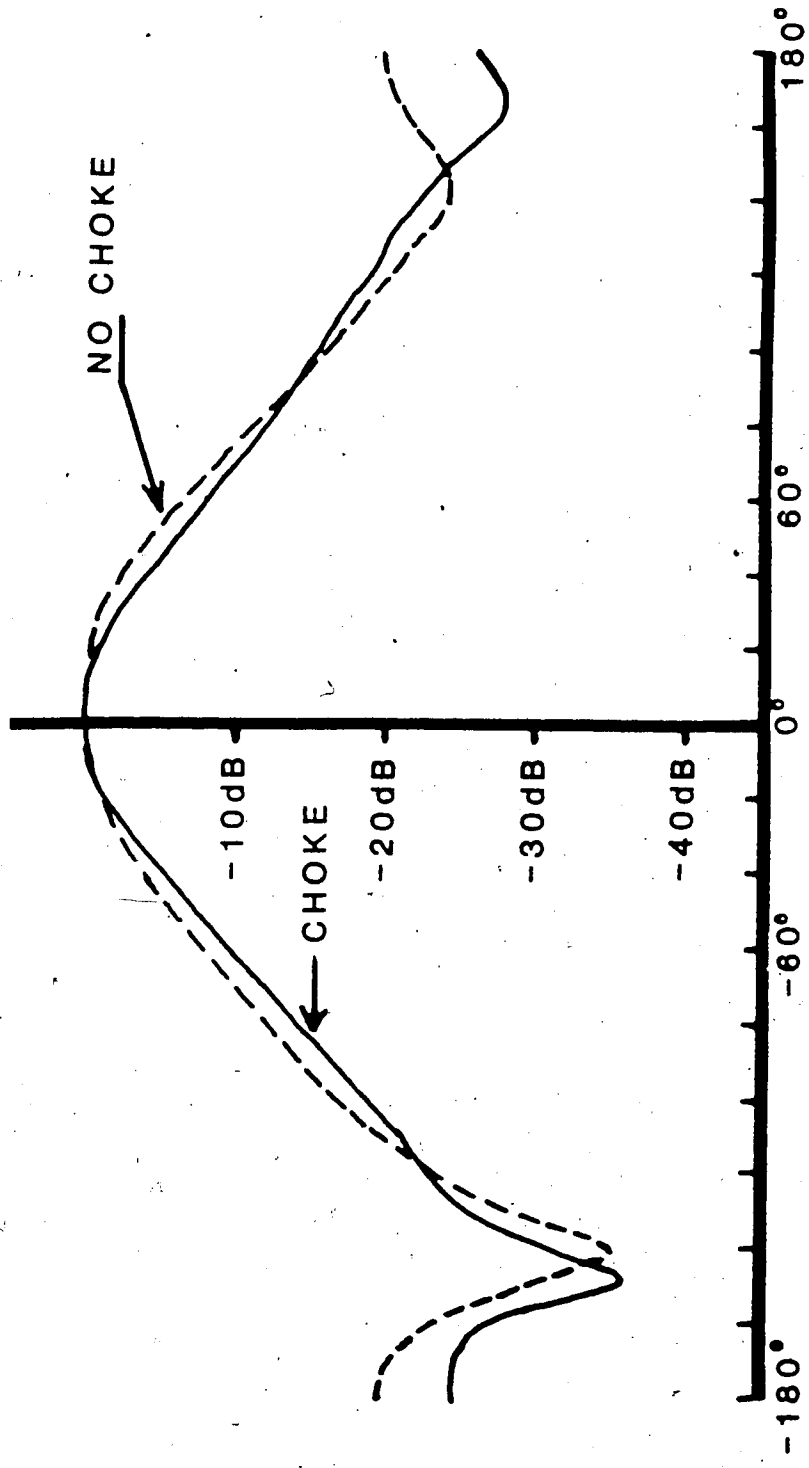
It is interesting to compare the antenna patterns of the 408 MHz feed horn with a cylindrical waveguide horn and a dipole array. The radiation patterns for a cylindrical horn with the same diameter as the dual frequency horn were calculated based on theory presented by Silver (1949). The calculated patterns are similar to those in Figure 2.6,

Plate 2.1

This photograph shows a dual frequency feed horn prior to installation on the dish. The outer choke ring is clearly seen. The four 408 MHz probes are within the large cavity. They are supported at each end, with the inner end insulated from the metal with a Teflon rod. The two inner rings set up the proper coupling at 1420 MHz between the flared waveguide and the large cavity for the optimum 1420 MHz radiation pattern. The innermost ring is connected to the circular waveguide.



E-PLANE



Radiation Patterns of Feed Horn at 408 MHz

Figure 2.6a

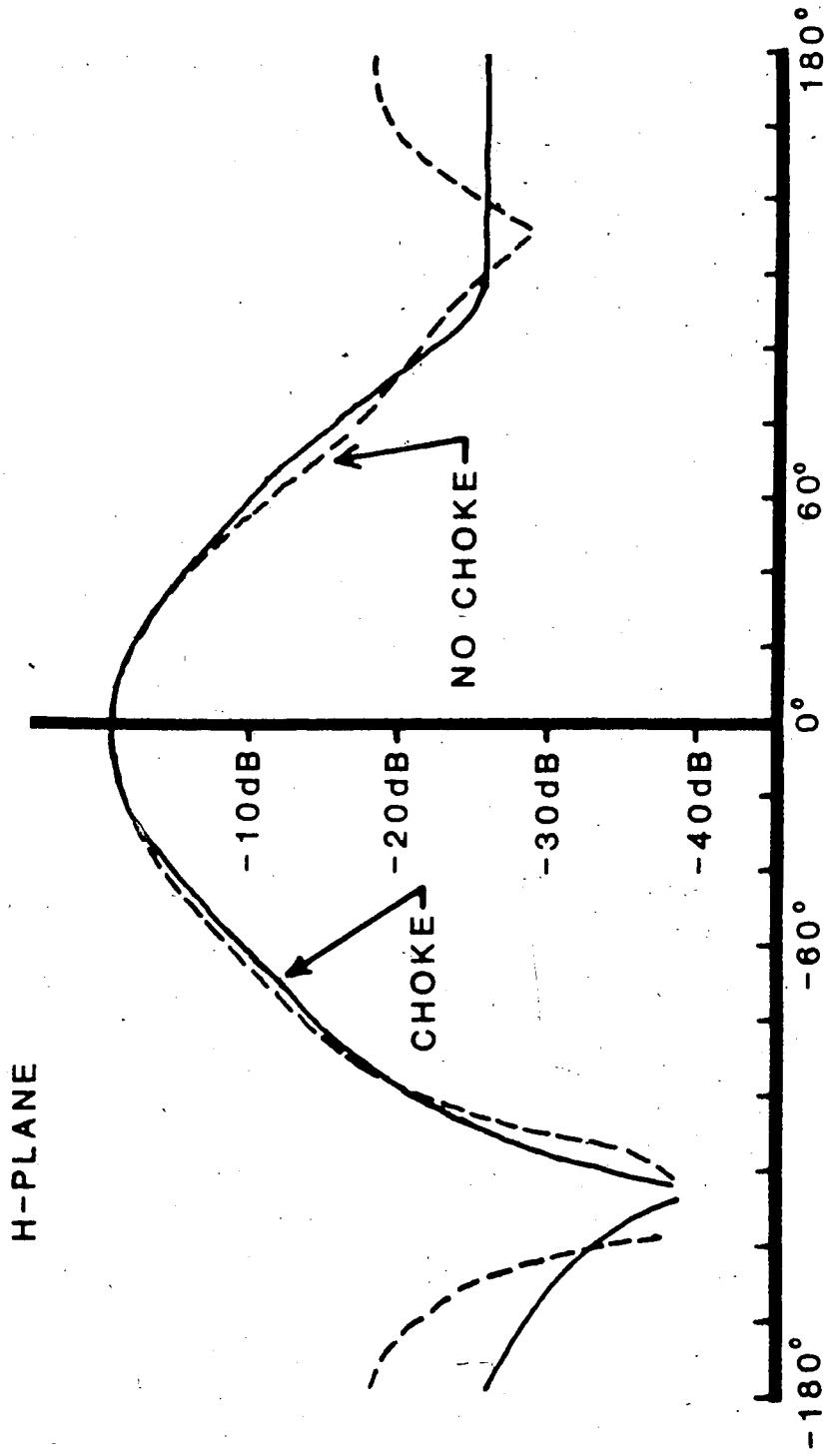


Figure 2.6b

except that the edge illumination is greater: -6 or -7 dB compared with -10 dB. A boxing ring antenna also has a similar simple pattern, but edge illumination is between -18 (E plane) and -12 dB (H plane). It appears that the dual frequency horn is a compromise between a cylindrical horn and a boxing ring array. This is reasonable because the cavity is so short that the structure is in a transitional stage between a pure antenna array and a pure waveguide horn.

D. Combining Network

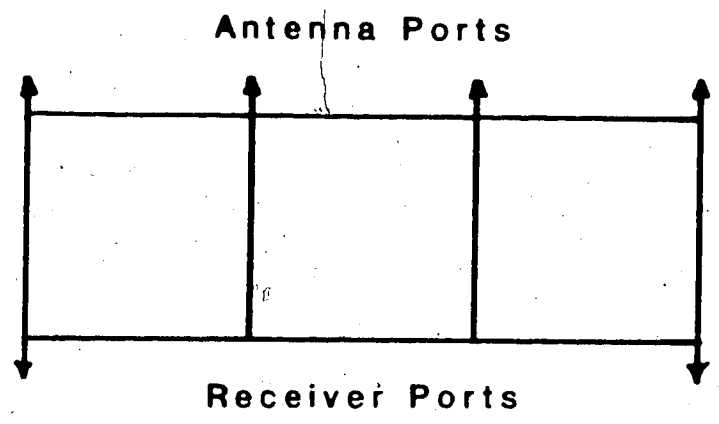
The last component of the feed to be discussed is a combining network that phases the four probes properly. Opposing probes must be fed in antiphase so that the electric field vectors set up in opposite sides of the feed cavity are coparallel, and the phase difference between orthogonal probes must be 90° so that circular polarization is received. A six-port device described by Saleh (1981) was used.

This network has appealing structural symmetry and simplicity; ten $\lambda/4$ 50Ω transmission lines are arranged in a ladder structure. The load impedances are also 50Ω . The four junctions on one side of the ladder are the antenna ports, and the junctions at the two corners on the other side are the receiver ports. The phase difference between two adjacent antenna ports is 90° , and the sign of the phase depends upon the receiver port used. Thus one port supplies right-hand circular polarization, and the other supplies left-hand circular

polarization. The phase and amplitude characteristics of this device are summarized in fig. 2.7.

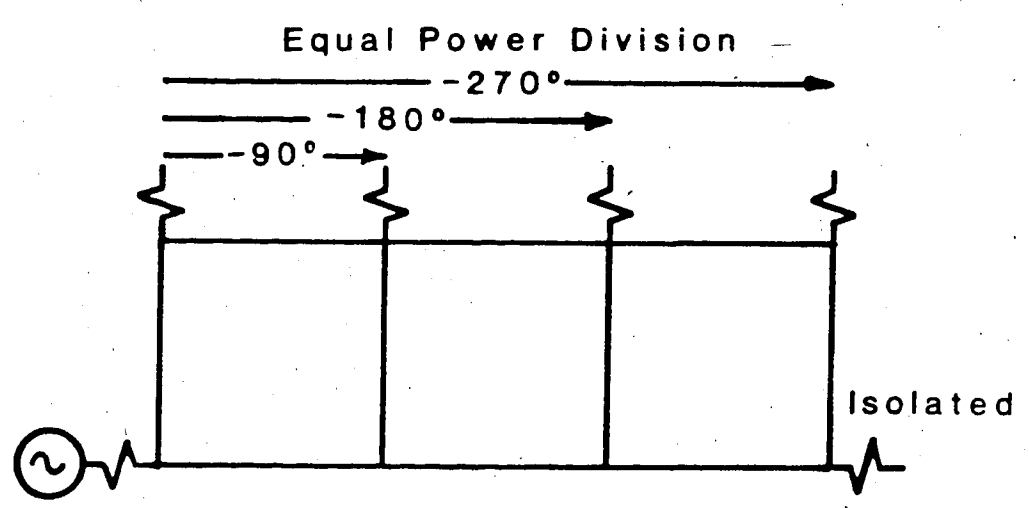
There are several subtleties in the operating characteristics of this device that should be mentioned. This device is really a special four-way power splitter/combiner. Power applied to a receiver port is equally divided among the 4 antenna ports, with 90° phase steps from port to port. Power applied to a single antenna port is also split equally four ways. Each receiver port receives $1/4$ of the power, as do each of the adjacent ports, but with equal phase. If independent sources are attached to all of the antenna ports, this power division scheme remains true. Thus if each source supplies equal power then each receiver port receives that same amount of power, namely one quarter of the power from each of four antenna ports. The remaining power is dissipated in the sources. This is significant because it means that if four independent, equal intensity sources are connected to the four input ports, the output is the same as if the network had only one source and one input. This is an important result for the noise measurements to be described later.

Sources in the sky provide coherent sources. Opposing probes supply signals with a 180° phase difference to two ports separated by a third port. This middle port receives an equal fraction of the power from the two other ports, which each undergo identical phase shifts, and arrive out of phase. Therefore the signals cancel. This power



All coaxial cable lengths between junctions are $\lambda/4$. Cable characteristic impedance equal to load impedances. At junctions, centre conductors joined together and shields joined together.

Combining Network Construction



Amplitude/Phase Characteristics

Figure 2.7 Antenna Combining Network

appears in the receiver ports. The distribution of the power between the two receiver ports will depend upon the polarization characteristics of the celestial source. With a randomly polarized source or linearly polarized source, the power is equally divided between the two receiver ports, since the wavefront can be decomposed into two circularly polarized components of equal intensity. If the source is partly or wholly circularly polarized, then one port receives more power than the other.

The network was constructed of $\frac{1}{4}$ " diameter semi-rigid coaxial cable. Since phase shifts were obtained through time delays, the network was frequency sensitive. In addition, because of slight variations in cable lengths and network construction, the phase differences between pairs of antenna ports were not the same, nor precisely 90° . The lengths used were therefore cut by an iterative process.

Deviation from 180° between opposing probes results in steering the feed radiation off axis. Using trigonometry and invoking a $\sin(x) \approx x$ approximation, it can be shown that this phase or delay error (d) slews the antenna pattern by:

$$\theta \approx 11 \frac{d}{s} \text{ [degrees]}$$

If the spacing, s , between the probe feed points, is 55 cm, the equation becomes:

$$\theta \cong \frac{d}{5} \text{ degrees}$$

with the phase error d expressed in degrees. The worst measured error at the band edge was 5° , which means that the feed will be pointing about 1° off centre. This is a trivial amount since the reflector subtends 120° at the focus.

The accuracy of the 90° phase shift determines the feed's response to circularly polarized radiation. The most common description of circular polarization uses two electric field vectors, both temporally and spatially in quadrature. Mathematically this can be written:

$$\begin{aligned} E(t) &= A \cos \omega t \mathbf{a}_x + A \cos (\omega t - 90^\circ) \mathbf{a}_y \\ &= A \cos \omega t \mathbf{a}_x + A \sin \omega t \mathbf{a}_y \end{aligned}$$

with \mathbf{a}_x and \mathbf{a}_y designating orthogonal unit vectors perpendicular to the direction of propagation. Now suppose that there is a phase error of ϵ . This error can be evenly distributed between the x and y components:

$$E(t) = A \cos\left(\omega t - \frac{\epsilon}{2}\right) \mathbf{a}_x + A \sin\left(\omega t + \frac{\epsilon}{2}\right) \mathbf{a}_y$$

Using trigonometric identities and rearranging:

$$E(t) = A \cos \frac{\epsilon}{2} [\cos \omega t \mathbf{a}_x + \sin \omega t \mathbf{a}_y] + A \sin \frac{\epsilon}{2} [\sin \omega t \mathbf{a}_x + \cos \omega t \mathbf{a}_y]$$

The left hand term represents a counter-clockwise rotating vector, and the right hand term represents a clockwise rotating vector. For small errors the relative response of the feed to the unwanted sense of

polarization is

$$R = \frac{\sin \frac{\epsilon}{2}}{\cos \frac{\epsilon}{2}} \cong \sin \frac{\epsilon}{2} \cong \frac{\epsilon}{2}$$

$$\cong \frac{\epsilon [\text{deg}]}{120}$$

If the error is 5° , then the ratio of the field amplitudes is $1/24$ or about 0.04 or -27 dB. In practice this ratio will be better, since the above worst-case value is only a spot value at the edge of the band. The receiver uses broadband noise and spot values away from this band edge will have a smaller R .

So far only the phase response of the combining network has been discussed. The amplitude response, or the network losses, are also very significant since the signal power is multiplied by a factor α , and noise power equal to $(1-\alpha)kTB$ is added. By measuring the noise added to the network by a resistive noise source, the loss was determined.

A Dicke total power receiver was used to measure the losses of the combining network and the cables that join this network to the feed horn. A well matched termination immersed in liquid nitrogen was used as a noise source. This load was used because its noise temperature was not excessively large compared with the increase in noise due to the device under test. Consider the measurement of the losses in the coaxial cable (0.73 metres of RG-214) that runs from a probe to the network. First, the temperature of the load alone was measured with the Dicke receiver. Next the cable was placed between the load and receiver and the temperature measurement was repeated. The loss of the

cable was then determined using this set of equations:

$$T_1 = T_{\text{load}}$$

$$T_2 = \alpha T_{\text{load}} + (1-\alpha)T_{\text{ambient}}$$

Each of these cables has 0.09 dB of loss and thus adds 6K of noise. To measure the losses of this network it was necessary to connect cold loads to each input. Since these are independent noise generators, these 4 ports with 4 loads behave like a single port and a single load, and the measurement technique is the same as with the piece of cable. The loss of the network was found to be 0.04 dB, which increases the noise temperature by 3K. The total contribution of the network and cables is 0.13 dB or 9K.

These numbers are similar to those obtained by multiplying the cable lengths by the specified loss per unit length. For both RG-214 cable and $\frac{1}{4}$ " O.D. semi-rigid coaxial cable the loss is 0.15 dB/metre. The calculated loss for 0.73m cable is 0.11 dB. The combining network is made of 10 pieces 0.13m long, so the average path length from antenna port to receiver port is $10 \times 0.13 / 4 \approx 0.3\text{m}$ and the average loss is 0.05 dB.

The feed and combining network have so far been treated separately; now they will be considered as a unit, for the characteristics of one device can be affected by the properties of the other. A good example of this is the isolation of one receiver port

from the other, which depends upon the quality of the match of the loads on the antenna ports. With 50Ω resistive terminations on the antenna ports, the isolation is greater than 35 dB from 400 to 418 MHz. However, the feeds do not have as high a return loss as the loads, nor do they have a high level of mutual isolation. These result in power being reflected back into the network. One way to understand what occurs with a reflection at the base of the probes is to replace this feed with an ideal feed behind a partially reflective plane. A circularly polarized wavefront is generated by transmitting through the antenna. Part of this wave is reflected, and the reflection changes its hand of polarization, thus the reflected power must end up in the port other than the one connected to the transmitter. The measured isolation is greater than 10 dB between 398 MHz and 412 MHz and averages 13 dB in a 4 MHz band centred on 408 MHz. This means that the system temperature of a receiver connected to one port will increase by a fraction of the equivalent noise temperature of the load on the other port. 13 dB translates to a power ratio of 1/20, so an ambient temperature load increases the system temperature by $300/20$ or 15K, and a GaAsFET low noise amplifier ($T_{input} \approx 70K$ measured) used as a load (Frater and Williams 1981) produces an increase of $70/20$ or 3.5K.

This effect also makes the match to the probes appear better than it actually is. This is because the network tends to divert power reflected by the loads away from the source, as explained above. The measured return losses for the feed horn with combining network is

shown in Fig. 2.8 for both hands of polarization. Comparison to the single probe return loss in Fig. 2.5 will show the dramatic improvement in matching due to the network.

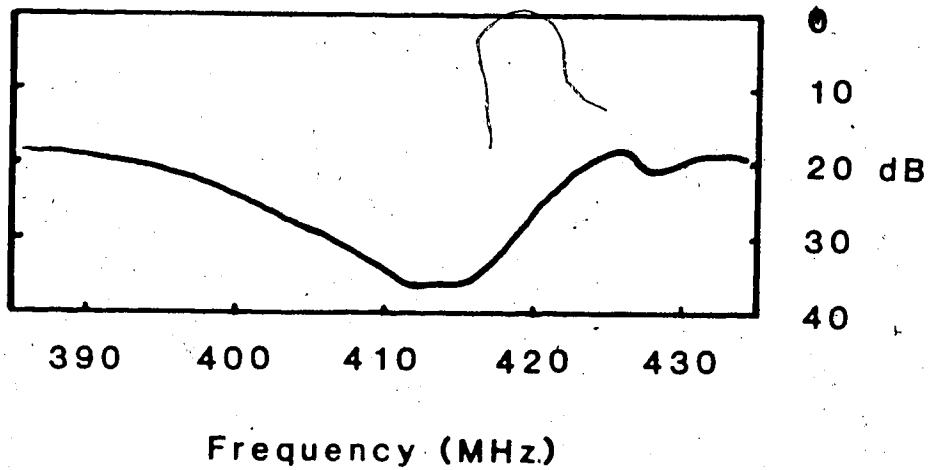
E. Frequency Independence Measurements

One of the most important specifications for the dual-frequency modification was that degradation of the primary frequency characteristics was unacceptable. A number of measurements indicate that the 408 MHz modifications have no significant effect on the 1420 MHz performance.

To determine if the 408 MHz feed structure modified the 1420 MHz field distribution, the 1420 MHz radiation patterns were measured with and without the 408 MHz probes. Small changes in the edge illumination were observed, but the magnitude of these changes was of the same order as the difference between repeated pattern measurements, with identical feed configurations.

Another way to measure the interaction between the two sets of probes is to measure the transmission from one set to the other set. The attenuation at 1420 MHz for a signal path from the 408 MHz probes through the 408 MHz combining network into the 1420 MHz probes was greater than 26 dB. Thus noise from the 408 MHz system will be reduced by at least a factor of 500 when it reaches the 1420 MHz receiver. At

RHCP



LHCP

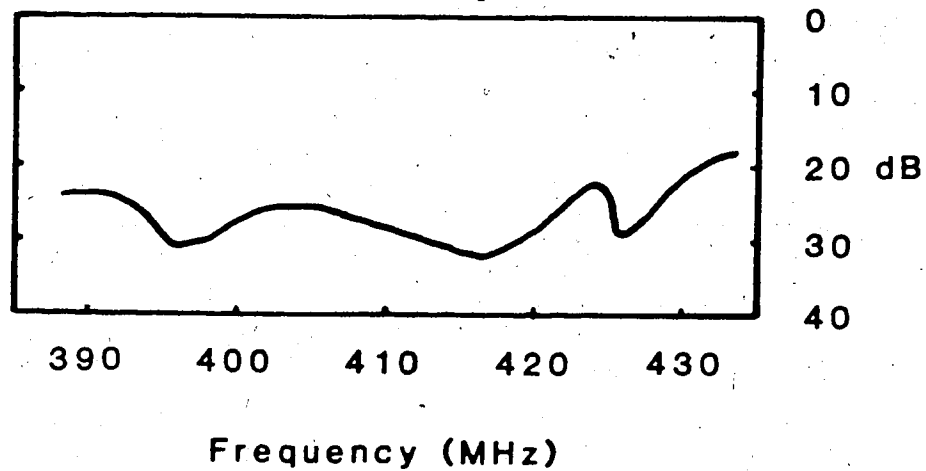


Figure 2.8 Return loss of entire feed system: feed horn, cables, and combining network. Each receiver port was measured with the other port terminated.

1420 MHz, the effective noise temperature of a 408 MHz GaAsFET LNA input is about room temperature and the increase in system temperature should be less than 0.6K.

Another way that coupling can occur is if waves coming out of the waveguide are reflected back into the waveguide by the 408 MHz probes. This possibility was tested by injecting a signal into one 1420 MHz probe, and measuring the coupling into the other probe. Because of the quarter-wave plate, a circularly polarized wave is launched, and any reflection would change the sense of rotation and emerge from the other probe. The coupling was measured both with and without the 408 MHz probes in place. This was found to be -18 dB and -19 dB respectively which is an insignificant change.

So far no mention has been made of coupling from the 1420 MHz probes into the 408 MHz probes at a frequency of 408 MHz. Since this frequency is below cutoff for the 14.95cm diameter waveguide, this interaction should be extremely small.

F. Performance on Dish

The most important test of a feed is to place it on a reflector antenna (see Plate 2.2) and to measure the performance of the combination. Characteristics that can be measured are the antenna pattern, aperture efficiency and spillover. The antenna pattern or primary pattern determines the area of the sky -

known as the field of view - that can be mapped in one survey. The aperture efficiency is a measure of the sensitivity of the dish. This is determined partly by the radiation pattern of the feed antenna. Spillover is response of the antenna to sources outside the main beam (primarily thermal radiation from the ground) via a direct path to the feed that does not include the reflector surface. These measurements were made using standard techniques involving a Dicke switch total power receiver and astronomical sources.

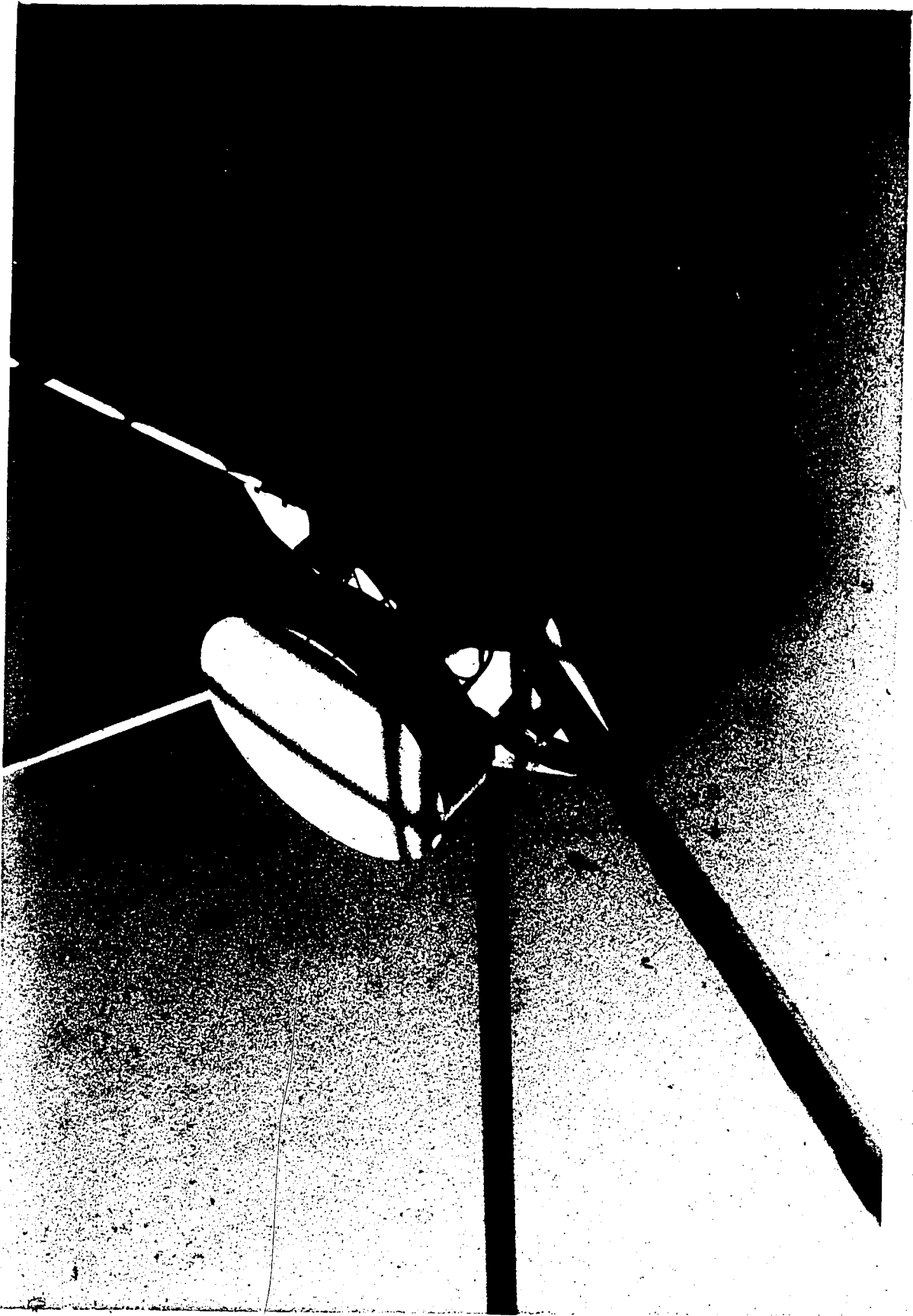
1. Dish Radiation Patterns

The antenna patterns were measured in two principal planes: declination; which involves scanning the dish in a north-south direction; and right ascension, which requires either mechanically scanning the dish east-west, or allowing the earth's rotation to sweep the beam through the test source. The test sources were Cassiopeia A, a supernova remnant which is a bright centimeter-wave source, and the sun. The large signal-to-noise ratio for these sources permitted the pattern to be measured rapidly and accurately. The half-power points were found to be separated by 5.3° in both right ascension and declination planes. The power response of the Far West dish in the declination plane is illustrated in Figure 2.9.

PLATE 2.2

FOCUS BOX

This box contains the receiver electronics. In front of the box, at the prime focus, is the feed. The box is insulated and temperature controlled to keep the electronics at a constant temperature. On the right-hand side of the box is the thermoelectric heater/cooler device. Several cables can be seen running from the back side of the horn into the focus box. These carry the signals from each 408 MHz probe to the combining network inside the box. The 1420 MHz signals enter the box via the circular waveguide. The cables running along the support legs to the side of the box carry LO and IF signals as well as power and monitoring signals.



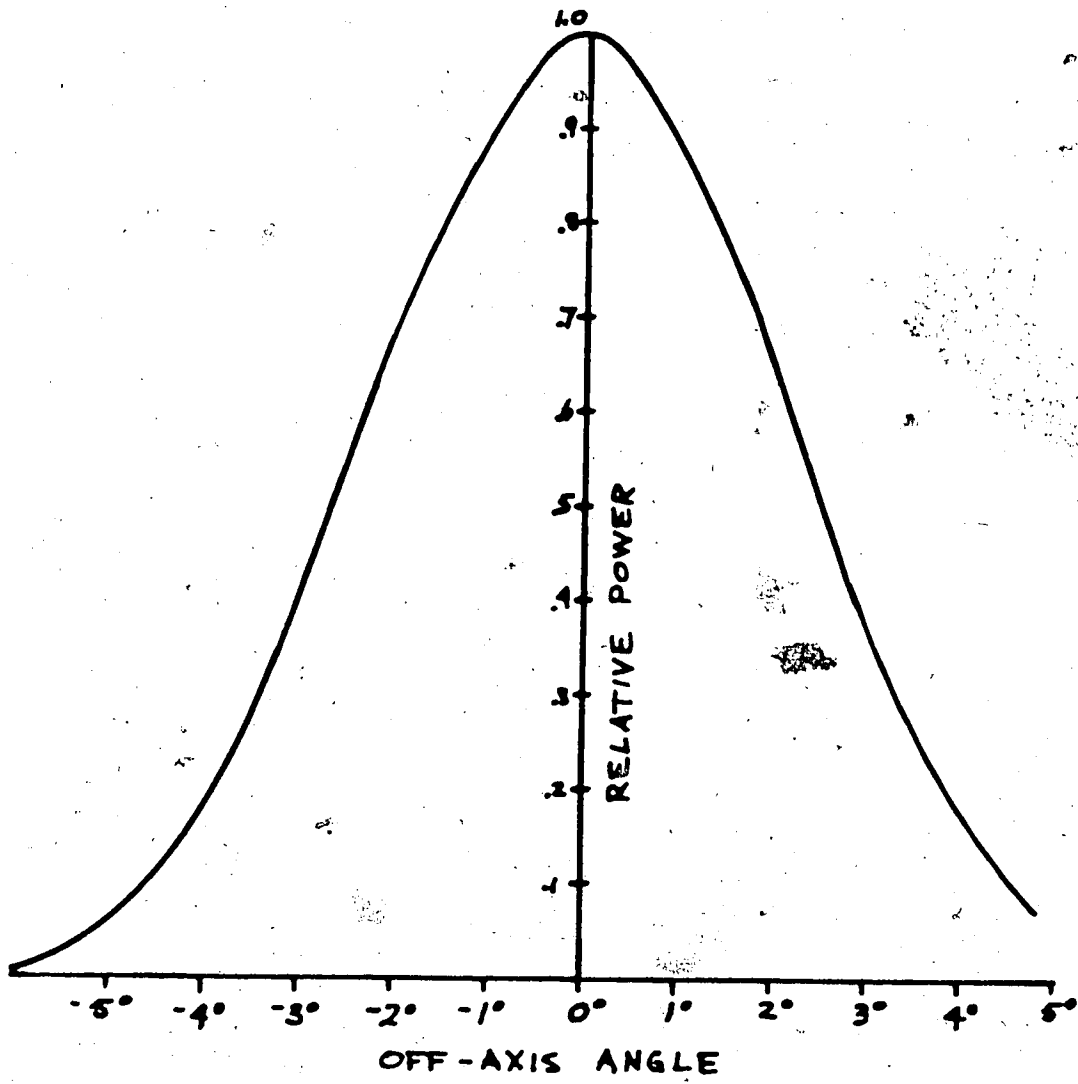


Figure 2.9 408 MHz Primary Radiation Pattern

2. Aperture Efficiency

The aperture efficiency is simply the ratio between the power out of a receiver connected to the actual antenna and the power out of the same receiver connected to an ideal antenna of the same cross-sectional area that delivers all the energy that it intercepts to the receiver. Again, Cas A was used as a test source. The flux was calculated using information from Baars et al. (1977). The efficiency was found to be 60% at 408 MHz and 54% at 1420 MHz.

The relatively high efficiency at the low frequency is probably another result of the shape of the feed pattern. At 408 MHz, the edge of the dish is illuminated more strongly than at 1420 MHz, so more of the collecting area is utilized and the higher efficiency results. The 1420 MHz efficiency is very close to that measured with a prototype feed without the 408 probes. This is further confirmation of the isolation between the two receiving frequencies.

3. Spillover

The spillover measurement involved an absolute measurement of the power out of a combining network antenna port with the antenna pointing at the zenith (at empty sky). The temperature scale of the receiver output was calibrated with precision 50Ω terminations at liquid nitrogen (78K) and boiling water (373K) temperatures. Then known

losses and sources of noise were subtracted to obtain the amount of noise due to spillover. This calculation follows:

T	(typical)		85K±1K
zenith			
Galaxy (typical) (Pauliny-Toth and Shakeshaft 1962)			-21K±2K
Antenna Losses:			
Unused port	15K±1K		
Combining network	3K±1K		-24K±2K
Cables	6K		
Solar noise			-10K±5K
Spillover			30K±10K

In practice the zenith antenna temperatures will be lower than those given here. The load on the unused receiver port couples to the receiver input via the combining network, increasing the system noise temperature. When these measurements were made, this port was terminated with a 50Ω dummy load at ~300K, but it is now terminated with a room temperature GaAsFET amplifier. The effect of this amplifier is the same as that of a termination at 70K. Thus the contribution of the unused port will drop from 15K to 3.5K, and the zenith temperature will be at least 73K.

The antenna temperature was also measured at elevation angles ranging from near zero (pointing at the horizon) to 90° (pointing at zenith). The sky contribution to the antenna temperature obtained from Pauliny-Toth and Shakeshaft (1962) was then subtracted at each of these points. The antenna temperature was constant within ±3K until the antenna beam neared the horizon, where it began to increase. When the dish was stopped by the horizon limits in the pointing mechanism, the antenna temperature had risen by 3K.

G. CONCLUSION

The 1420 MHz feed horn has been successfully modified to simultaneously receive 408 MHz radiation. This was done without noticeable degradation of 1420 MHz performance.

The performance of the antennas at 408 MHz can be summarized:

HPBW = 5.3°

Antenna temperature (less sky) = $52\text{K} \pm 4\text{K}$

Spillover = $30\text{K} \pm 10\text{K}$

Aperture efficiency = 60%

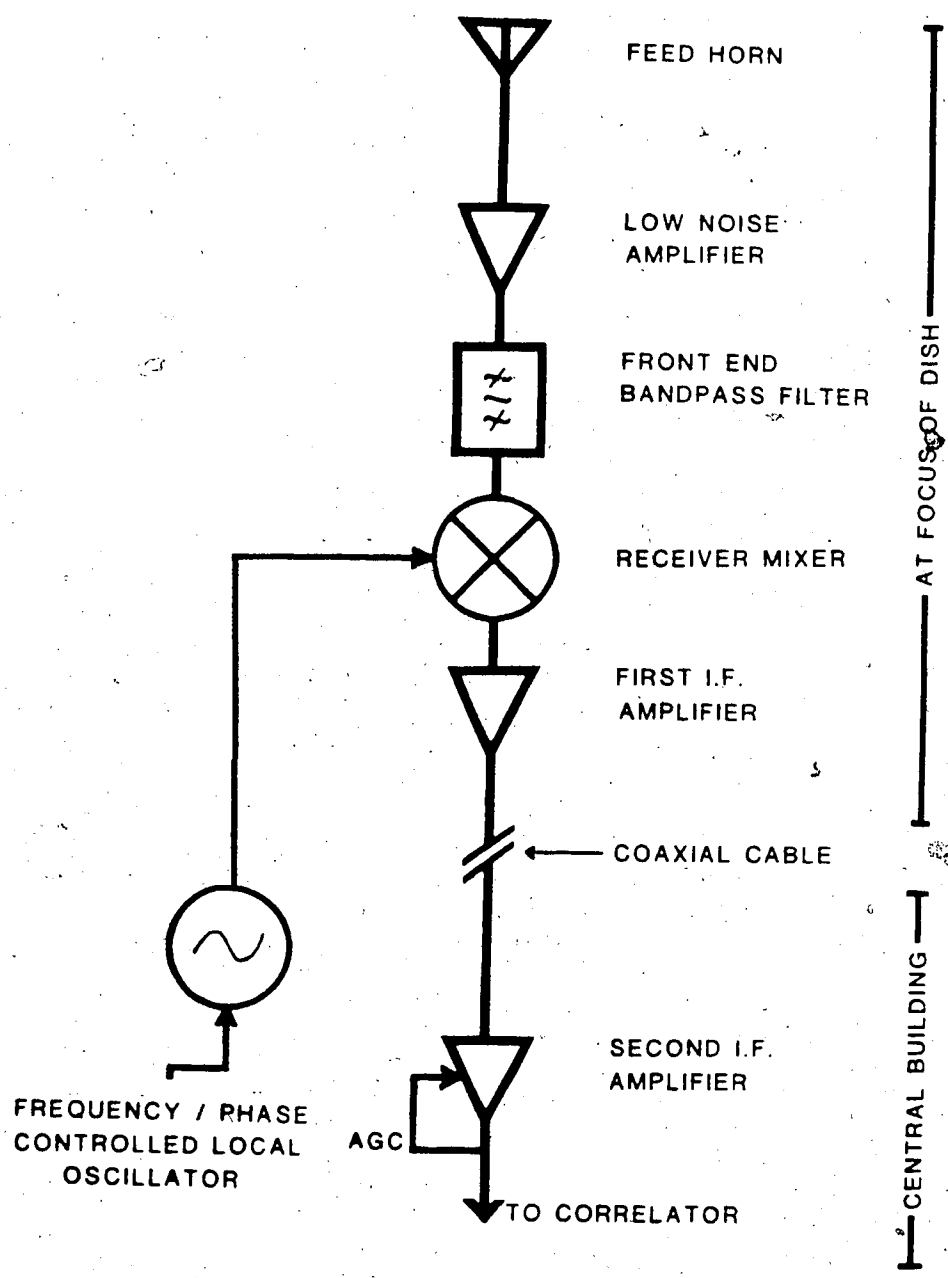
Bandwidth \cong 20 MHz

CHAPTER 3: 408 MHZ RECEIVER

A. The General Problem

The problem that was set before me was to develop four parallel receivers that are sensitive enough for radio astronomy applications and also stable enough to be used to produce images of the sky. The need for sensitivity is obvious: the receiver-generated noise must not be large enough to overwhelm the signals from weak sources in the sky. The stability - amplitude and phase - requirement is necessary because of the way that the images of the sky are made. As explained earlier, the sky is sampled by the interferometer fringes. The visibilities or Fourier components not only depend upon what is in the sky, but also the amplitude and phase characteristics of the receivers. When the image is formed by summing the Fourier components, if the amplitudes and phases of the receivers are not what one believes them to be, the image will not be constructed correctly. Each of these areas of concern - sensitivity, gain stability, and phase stability - will be discussed separately and explained below.

First, the major building blocks of a radio astronomy receiver will be outlined. A very basic receiver is shown in fig. 3.1. Remember that an interferometer requires at least two of these receivers. The problem is to make each receiver operate in a very similar manner with respect to all the others. What makes the



BLOCK DIAGRAM OF A RADIO ASTRONOMY RECEIVER SUITABLE FOR USE IN AN INTERFEROMETER

Figure 3.1

situation more difficult is that the receivers are in separate enclosures and run from separate power supplies. In spite of this, several control systems can be used to stabilize the receiver. These circuits were one of the main areas of interest of this project.

After the signals from the sky are collected by the feed horn, they are amplified by a low noise amplifier (LNA). Contrary to common communications receiver design principles, the front end bandpass filter follows the first stage of gain. It is very important to maintain a high signal to noise ratio, and loss before the first stage of gain would result in an increase of noise. Communications receivers often place filters preceding any gain because they are tuned to frequency bands that have many strong carriers. Without the filter, the front end amplifier might be pushed into saturation by a strong signal. This could desensitize the receiver or produce spurious signals through intermodulation in the amplifier. The increase in system noise is often not as important with communications receivers, because of the greater signal levels of man-made radio sources. Near the 408 MHz observing band are several frequencies used by both terrestrial users and satellites. For this reason the design of the front end had to take into consideration potential man-made interference.

Following the LNA and filter is a mixer which converts a band of signals centred on 408 MHz to a band centred on 30 MHz, the

intermediate frequency (IF). A commercial double balanced diode mixer was used here.

The IF amplifier frequency is 30 MHz. The signal frequency is nominally 408 MHz, so an LO frequency of 378 MHz was chosen. A signal at 348 MHz will also produce a 30 MHz output, but the input filter rejects this "image" frequency.

A tuned IF preamplifier follows the mixer. Commercially available amplifiers are used since some very high quality units are available, and considerable effort would be required to build an amplifier that would be equal in performance. The IF preamplifier is placed preceding the cable to compensate for the cable losses and hence maintain a low system temperature.

After travelling down the transmission line to the Synthesis Telescope building, the IF signal is again amplified. This IF amplifier has higher gain and a narrower passband than the previous stage. In addition, its gain can be controlled with a voltage. A portion of the output is sampled and rectified, and processed to provide a voltage to adjust the gain to keep the output power constant. If the input power to the receiver is constant, a reasonable assumption since the dishes point at the same area of the sky during the entire observation, then this automatic gain control (AGC) circuit will keep the receiver gain constant. The amplified IF signal is then

passed to the Digital Signal Processor (DSP) where it is correlated with signals from the other receivers (Lo 1982).

Local oscillator (LO) circuitry is located at both ends of the cable. This system makes the signal phase from sky to correlator entirely independent of the length of the coaxial cable connecting the antennas to the central receiver. This device is very important since the cable is not in a controlled environment like the rest of the receiver. It is subject to large and sometimes rapid temperature variations which change the cable length. Designers of other synthesis telescopes either attempted to control the cable temperature or else used a local oscillator that produced a constant phase to the mixer. This local oscillator is the first known system to stabilize the phase to the IF output. Because the Digital Signal Processor does the fringe derotation after correlation, the LO phase does not have to be continuously variable. It is switched in 180° steps to reject common mode errors. It is also switched 90° for calibration of the real and imaginary channels of the correlator.

The system design specifications for the 408 MHz receivers should now be stated:

- centre frequency of 408 MHz, tunable ± 3 MHz to avoid interference;
- 4 MHz IF bandwidth;
- low system temperature

- low susceptibility to man-made interference;
- very stable gain;
- stable phase characteristics;
- LO phase controllable in accurate 90° steps;
- subsystems must share a single coaxial line between antenna and centre of interferometer.

Now the design philosophy used will be set forth:

- the system engineered is not an experiment, it is a permanent addition to a research instrument, and was constructed with this point in mind.
- the new system must use existing observing and map production software with a minimum of modification.
- commercially available devices such as amplifiers and filters were purchased unless there was a definite advantage in constructing the device. The wheel has been invented one too many times.
- the use of necromancy was avoided, since the equipment will be repaired and possibly duplicated without my attention.
- everything was made as simple as possible, but not simpler (Einstein).

The development of this receiver will be discussed in four parts:

- the front end, the mixer and receiver sensitivity;
- the IF amplifiers and receiver gain stability;
- the local oscillator system and receiver phase stability;
- system tests.

The LO system design is unique and therefore many pages will be devoted to its development. Other subsystems are more conventional and were either commercially built or were developed by other workers, and thus will be covered in less depth.

B. Receiver Front Ends

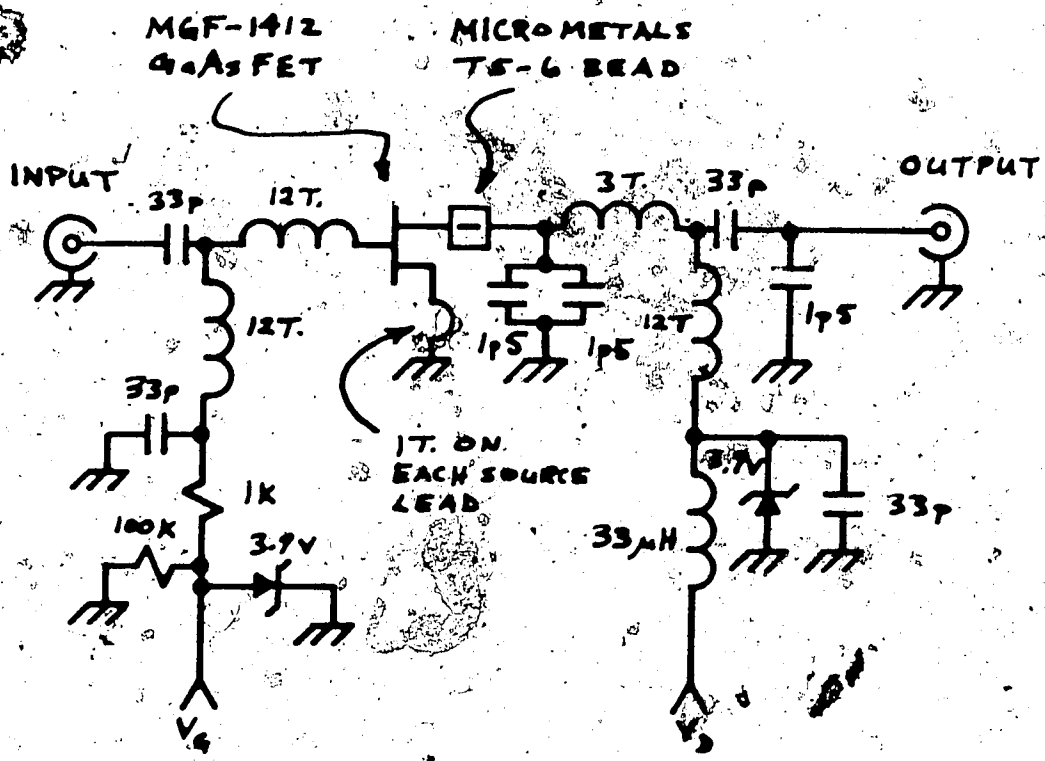
The 408 MHz front ends consist of two stages of low noise amplification separated by a bandpass filter. In the development of the front ends, low noise figure and good large-signal handling capabilities were of prime concern. This arrangement gives a system temperature of about 104K, 50K of which is due to the low-noise amplifiers.

Commercial low noise amplifiers (LNAs) constructed with bipolar transistors were originally purchased for the 408 MHz receivers. The specified noise temperature of these amplifiers was 120K, but all the units were tested and the noise temperature was found to be about 180K. This was too large to be acceptable. Unfortunately a manufacturer of a superior amplifier could not be found. However, 400 MHz is high enough

that $1/f$ noise becomes insignificant in gallium arsenide field effect transistors (GaAsFET) (Cooke 1982). At least one semiconductor manufacturer claimed to make GaAsFET devices with a noise figure of 0.5 dB or 35K at 400 MHz. In addition to the superior noise performance, GaAsFETs are much more linear than bipolar transistors and are thus less prone to intermodulation. A design existed for amplifiers built with GaAsFETs (Galt, personal communication) so it was decided to have a technician construct and adjust a set of amplifiers. This circuit is shown in Fig. 3.2.

In the adjustment of these amplifiers several factors and variables had to be considered. Of course minimum effective noise temperature and maximum gain were desired. The amplifiers also had to be stable for the loads that they would be attached to. To satisfy these requirements, the drain current and drain voltage were varied, as well as the input and output matching networks. As suggested by Weinreb et al (1982), a small inductance was placed between the source leads and ground to improve the input match (Anastassiou and Strutt 1974). With these particular LNAs the improvement was minimal.

One major problem encountered with this design was a tendency for the amplifier to oscillate in the vicinity of 4 GHz. The solution was to place a small piece of conductive foam near the input inductance. The foam is carbon impregnated and is often used to protect integrated circuits from static damage. The foam was kept small to minimize



ALL INDUCTORS #30 WIRE ON 0.215 CM FORM.

Figure 3.2 GaAsFET Low Noise Amplifier

losses at 408 MHz, yet large enough to reduce the gain at the higher frequencies, stopping the oscillations. This lossy foam technique is akin to the use of ferrite beads, and other workers have had to resort to this method of amplifier stabilization. After this was done, I_D and V_{DS} were adjusted for optimum noise figure and gain. The stability was verified by subjecting the LNA to various loads that could be encountered in the receiver as well as open circuits and short circuits.

After discussion with the Department of Communications, and some interference monitoring, it became apparent that there would be man-made signals near the observing band. Thus the receiver was deliberately designed to be less sensitive to interfering signals with very little reduction in sensitivity to radio astronomy sources.

Additionally, radio astronomy receivers have been built with the LNA following the antenna and preceding the front end filters. If a loss precedes the LNA that attenuates the input signal by a factor α , the increase in noise temperature is $(1-\alpha)T_a$ where T_a is the physical temperature of the lossy device. T_a is usually about 300K. Most filters have an insertion loss of several decibels. Suppose that the loss is 2 dB or 0.63, then the increase in system temperature due to the loss is 110K, which is not acceptable for low noise receiving systems. Thus radio astronomy receivers usually have no filters before the LNA save for the frequency selectivity of the antenna. This

Unfortunately makes the front end very susceptible to out-of-band interfering signals.

The type of interference that was of most concern was intermodulation distortion. In a non-linear device, many possible combinations of these intermodulations are produced, and the danger is that two out of band carriers may generate a third signal within the observing band.

The noise figure was compromised slightly to obtain better protection from interfering signals by placing a filter between the two amplifier stages. The gain preceding the filter is 15 dB, and the increase in temperature due to the 2 dB filter loss is about 3K.

Although the first stage of amplification is subject to a wide band of signals, perhaps including strong man-made signals, the second stage receives only a select fraction of this spectrum, hopefully without interference. Without the filter, out-of-band signals may be amplified to a level by the first stage sufficient to cause intermodulation distortion in the second stage.

The question now arises concerning the amount of increase of noise that can be afforded. What is important is not simply the absolute increase, but the increase relative to other noise sources in the system. The system temperature, including the minimum galactic contribution, was found to be about 125K. If the location of the

filter has resulted in a change of 3K, then the signal to noise ratio has been reduced by 21%. It was felt that the slight increase in system noise due to the front end configuration was worth the added interference protection.

The performance of the front end low noise amplifiers consisting of two amplifier stages connected through a 408 MHz bandpass filter was measured. The typical noise temperature of these units at 408 MHz was $50\text{K} \pm 10\text{K}$. The bandwidth between the points where the noise temperature rises to 80K was typically 15 MHz. The gain of the sets of amplifiers varied between 25 and 33 dB, depending on the unit tested. The insertion loss of the input and output ports averaged 14 dB.

An interesting property of low noise amplifiers is that the equivalent noise temperature of the input can be lower than the physical temperature of the device (Percival 1939, Frater and Williams 1981, Forward and Cisco 1983). The noise power emerging from the inputs of the LNAs was measured and found to be equivalent to a resistive load at 70K. Extra amplifiers were constructed and used as loads on the unused receiver port of the feed combining network. Since the amount of coupling between the used and unused receiver ports is $1/20$, changing the load temperature from 300K to 70K has reduced the noise added to the system from 15K to 3.5K. With a system temperature of 104K, this means that the signal to noise ratio has been improved by about 10%.

A readily available commercial mixer was used for the receiver mixer. The device is a double balance mixer with a ring of four diodes. The conversion gain is about 1/4 or -6 dB with a local oscillator signal power of 5 mW or +7 dBm. The IF output of the mixer goes to the IF preamplifier stage.

The sensitivity of the synthesis telescope to a point source is an important statistic. Napier and Crane (1982) show how the following relation is obtained:

$$\Delta S = \frac{2\sqrt{2} k T_s}{\sqrt{Btc} \eta_c \eta_a A_a}$$

ΔS = noise power

k = Boltzmann's constant = 1.38×10^{-23} Joule/°K

T_s = system temperature = 104K

B = receiver bandwidth = 4 MHz

t = observing period = 12 hr.

c = number of correlations = 140 (for full survey)

η_c = correlator efficiency = 0.89

η_a = aperture efficiency of antenna = 0.6

A_a = antenna area = $\pi(4.5\text{m})^2$

For a full survey (140 spacings or 35 days) the rms noise is 2.4 mJy/beam.

C. Automatic Gain Control

Each visibility measurement of the sky consists of two numbers: the amplitude of the correlated signal; and the phase difference. If there is an error in the amplitude of the visibilities, then the strength of the mapped sources will not be known for certain. If this error varies with time, then the noise level of the map will increase since the Fourier components (or visibilities) will not add together in a way that tends to cancel the side lobes. Thus for the best map, the visibility amplitudes must be well known which is ensured if the receiver gains are kept constant.

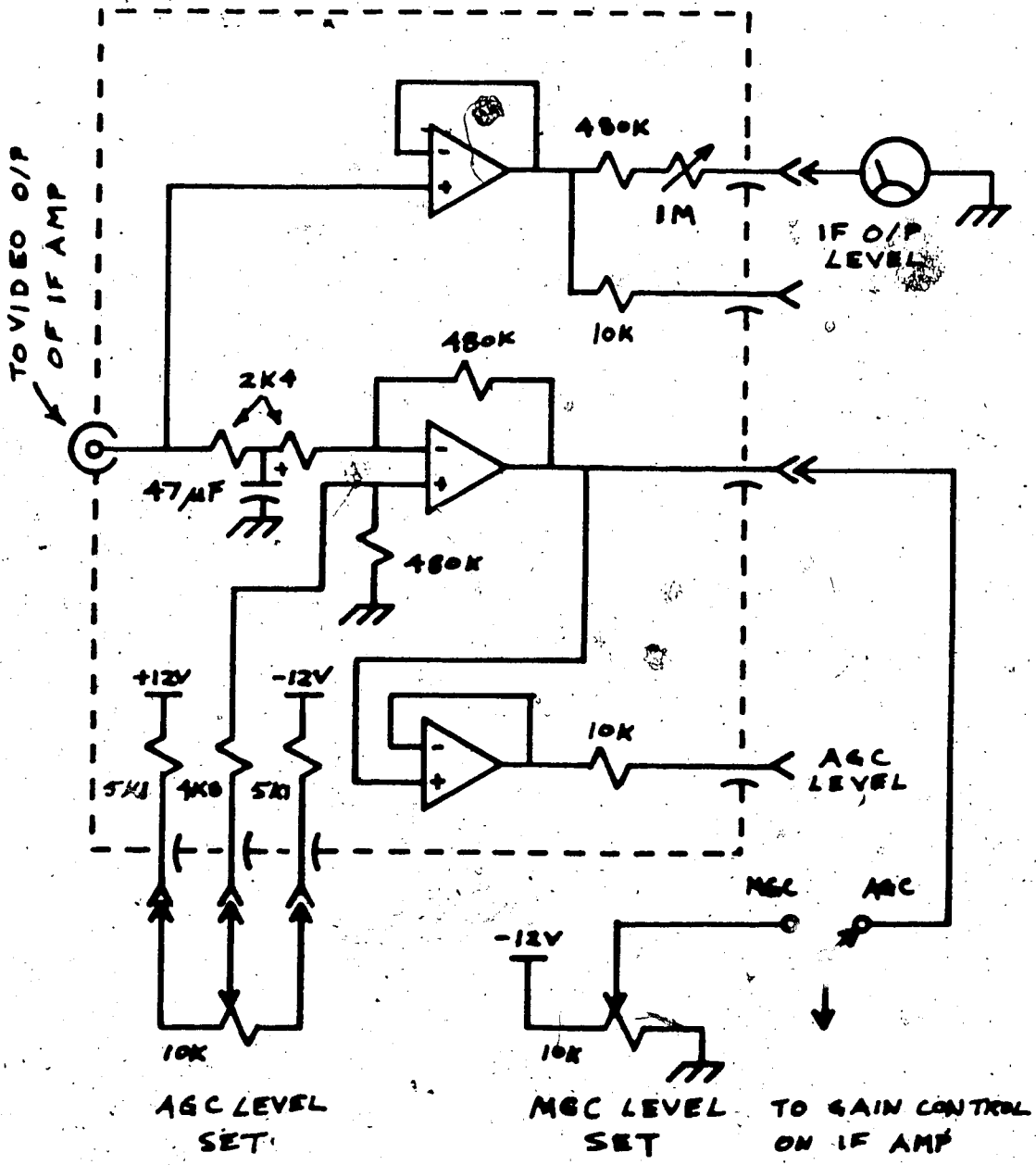
The maximum allowable error in the gain should be determined. Experienced interferometrists at Cambridge (Baldwin and Warner 1979) state that most interferometers are capable of a gain stability ($\Delta G/G$) of 1%, and that better amplitude stability would not be useful because it would be hidden by phase errors.

One way to control the receiver gain is to receive a signal of constant intensity, and adjust the gain to keep the output level constant. Fortunately, there is one such signal that is inherent to the system: the system noise. The receiver noise originates from many sources: the receiver mixer; the low noise amplifiers; losses in the cables to the horn, the combining network, and the horn itself; spillover; the galactic background; and the source being mapped.

Assuming that these stay constant, and that a reference voltage level stays constant, then a difference amplifier can compare the output level to the reference level and adjust the IF amplifier gain to counteract any changes in gain between the antenna and the IF amplifier's output.

The AGC circuit used is shown in Fig. 3.3. The IF amplifiers used have two outputs: an intermediate frequency output and a video (or rectified) output. The IF output goes to the correlator and the video output is used by the AGC amplifier. The amplitude of the video output represents the output signal level. This signal is filtered in an R-C circuit and is applied to the inverting input of an operational amplifier. The non-inverting input is connected to a voltage reference formed by an adjustable resistance wired into a voltage divider. The difference between these two inputs is amplified and is applied to the gain control voltage input of the IF amplifier. Thus this closed-loop tends to minimize the difference between the reference and the video output, keeping the IF output level constant.

The AGC itself creates a problem. It keeps the output power of the receiver constant irrespective of the brightness of the region being mapped. Thus the system gain will be different for sources that produce a different antenna temperature. This multiplies the source brightnesses in the map by a factor that is constant across the map. The intensity scale of the map can be calibrated by multiplying the map



OP-AMP : $\mu A741$

Automatic Gain Control

Figure 3.3

by the system temperature correction. This correction factor can be obtained by dividing the system temperature with a dish pointed at a region of the sky with a known temperature by the system temperature of the dish pointed at the mapped region.

Another reason to use an AGC circuit is to keep the rms input levels to the analog-to-digital conversion circuits, known as quantizers, constant. The input signals are quantized to one of three possible levels. The decision levels are fixed, so for meaningful quantization, the input must not be too large nor too small.

D. The Local Oscillator System and Phase Stability

1. Need for Phase Stability

Phase stability is essential for an interferometer of this type, for without it images of the sky with correct absolute positions of sources cannot be made. The prime source of phase error is changes of length of the coaxial cable transmission line due to temperature changes. The system developed controls the phase from the output of the LNA to the output of the IF amplifier in the Synthesis Telescope building. With this system the change in IF phase for a change in transmission line length is at least 7 times better than would be expected for a system that only stabilizes the LO phase, and at least 90 times better than a system with no phase stabilization.

The relative phase between receivers making up an interferometer determines the position of the fringes in the sky. A phase error changes the position of the fringes and results in a position error of the Fourier components that form the the map. Since a point source is actually the sum of many Fourier components, random phase errors will tend to blur the point source. Equally important, at locations where there is no source, the components must add to zero, but errors may lead to a non-zero sum, which means that the noise level of the map has risen. An equivalent way of looking at this is that the synthesized beam has been broadened and reduced in amplitude and that the side lobe level has been raised. This kind of phase error with a synthesis telescope is analogous to errors on the reflecting surface of a filled aperture radio telescope and the effects are the same.

The question of specifying the maximum phase error now arises. One might get an estimate by considering filled aperture radio or optical telescopes. The maximum allowable rms error with these instruments is often specified as $\lambda/10$. This corresponds to a maximum rms phase error of 72° . Before this is applied to a synthesis telescope, one very important point should be kept in mind. That is, in a filled aperture each spacing is effectively measured many times, while with most synthesis telescopes there is no redundancy and each spacing is measured only once. Thus in a filled aperture telescope, many measurements are added together and the phase errors tend to cancel, while with a synthesis telescope, there is only one opportunity

to measure the phase for one spacing, so the phase had better be right. Rahmat-Samii (1983) has calculated the radiation patterns for reflector antennas with random surface errors of various magnitudes. His results show a surface with $\lambda/10$ errors has a reduced main beam amplitude, -6dB in his examples, and increased sidelobe levels. He also shows that to maintain the correct sidelobe amplitude, the surface accuracy must be much better than $\lambda/10$. Dragone and Hogg (1963) have done a similar study, but out to higher order sidelobes. They show that to keep these sidelobe levels to within 3 dB of the ideal pattern the surface accuracy of the dish should be $\pm 0.01\lambda$ or $\pm 7^\circ$ in phase. This suggests that the peak-to-peak phase error in a synthesis telescope should be smaller than 14° to produce a beam with sidelobes that have small deviations from their ideal values.

It is useful to consider the phase stability requirements for other synthesis telescopes. Based upon experience at Cambridge, Baldwin and Warner (1979) have plotted expected phase error due to the ionosphere versus frequency and baseline. For a 600m baseline at 400 MHz, their expected rms error is about 1° . For the design of the Very Large Array in New Mexico, Napier et al. (1983) specify a phase error of 1° rms per gigahertz. Based upon considerations such as these, it was decided to make the phase of the 408 MHz receivers as accurate as possible, preferably less than 1° rms.

Larger phase errors can be acceptable if adaptive-optics techniques are used. This is done to produce maps from Very Long Baseline Interferometers consisting of antennas scattered around the world (Steer 1984). However, these methods rely upon a large number of simultaneous correlations and a small number of uncomplicated source structures in the field mapped. The 408 MHz system has only four simultaneous correlations and will be used to map complicated objects that fill the field so these image construction techniques are not appropriate. In addition, one of the original specifications for this system was that it would use the same observing techniques and data reduction programs as used for 1420 MHz observations which depend on accurate phase.

2. Sources of Phase Instability

It should be clarified here that the phase stability that is of concern is the differential phase between antennas. There are a large number of potential sources of differential phase errors in the interferometer - virtually every component. Filters, amplifiers, mixers and transmission line, all change the phase of signals passing through them. On the short term, the phase characteristics of these devices are stable. As they age, these characteristics may change, but these changes are corrected by the routine calibration observations. One source of rapid phase changes is rapid temperature change. If all parallel sets of components undergo the same temperature change, and if

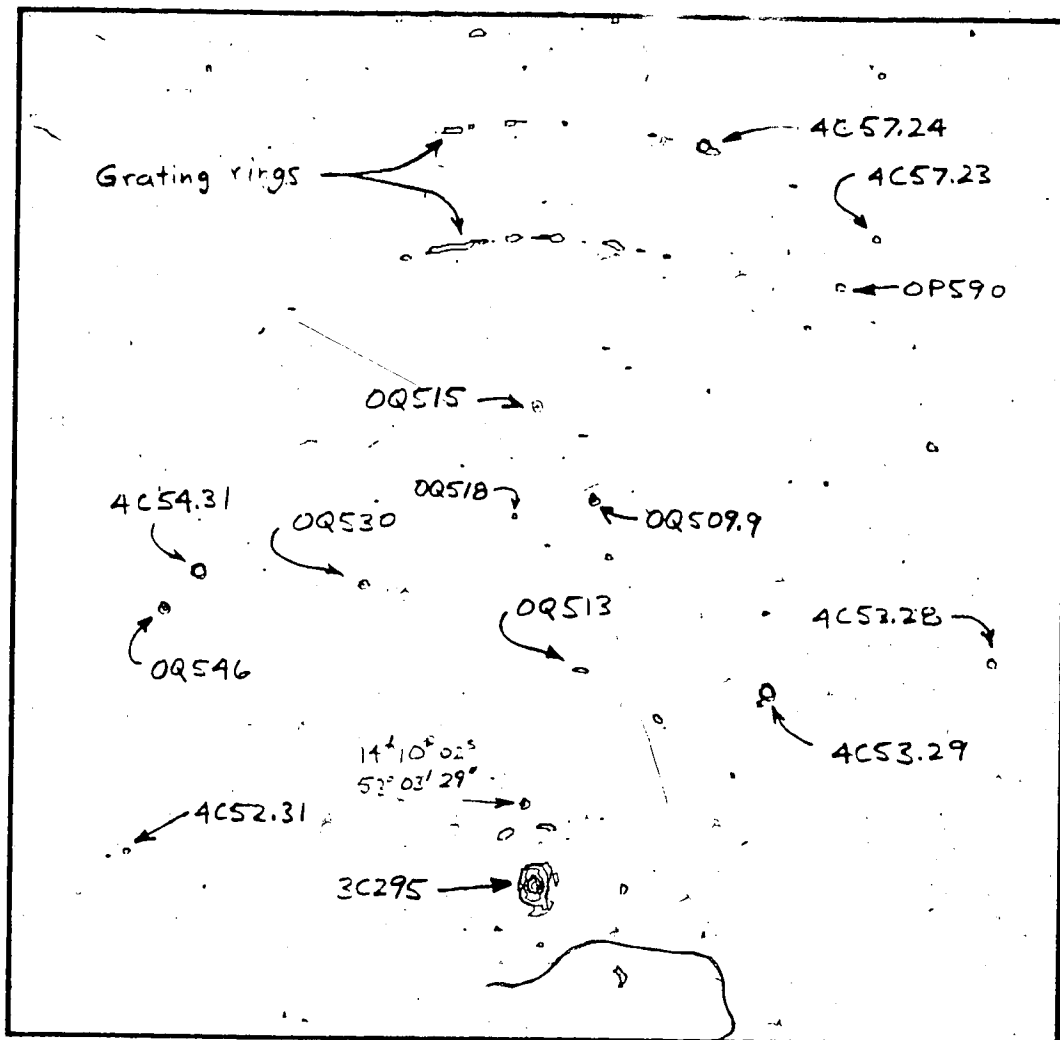
all the components have similar characteristics, the differential phase will not change. To establish this situation, all components were either constructed as similarly as possible, or specified to be phase tracking when ordered. In addition, the components were placed in constant temperature environments at the focus of the dishes and in the Synthesis Telescope building. The temperature control in the focus boxes is held to within 1°C of 26°C , and to within several degrees in the Synthesis Telescope building.

The coaxial cables running from the receivers on the dishes to the central Synthesis Telescope building are not at a controlled temperature, and the characteristics of different cables may not be exactly the same. Although the phase temperature coefficient is larger for the short lengths of RG-214, the phase change will be dominated by the much longer Helix cable. For a one degree increase in temperature, the phase of the output of the total cable length will change between -6° and -12° at 378 MHz, and it will change between $-1/2^{\circ}$ to -1° at 30 MHz. (The uncertainties are due to uncertainties in the manufacturer's specified phase temperature coefficient.) The frequency of 378 MHz was chosen because it is the ultimate local oscillator frequency. Even if a subharmonic of this frequency is sent down the cable, the phase gets multiplied along with the frequency when 378 MHz is generated, so the change in phase is the same as if 378 MHz were used. 30 MHz was also used in this illustration because it is the intermediate frequency. The phase change due to temperature would be

and 3.7 arcminutes in the east-west direction. The map encloses $7.4^\circ \times 7.4^\circ$ of the sky.

A second map of the 3C295 region was made, but with the map centre moved north 2.65° so that 3C295 was at the half-power point of the primary antenna pattern. The CLEANed map is shown in Figure 4.7 with identified sources labelled. The flux scale is the same as the previous map.

The amplitude of 3C295 on this map is 8800 units, which is .4 of the field-centre intensity. However, one would expect it to be .5 times the field-centre intensity since it is at a half-power point of the primary beam. This discrepancy is due to a phenomenon known as radial smearing which is analogous to chromatic aberration in optical telescopes. Radial smearing occurs because the effective array size is a function of frequency which in turn means that the map radial scale is a function of frequency. Since broadband noise is received by the telescope, a point source in the sky will produce a point on the map only if it is at the centre of the map, otherwise the source on the map is broadened in a radial direction from the centre. Since the flux is spread over a greater area on the map, the peak intensity is less. If the beam is assumed to be Gaussian, then from a graph plotted by Thompson (1982) it can be estimated that the peak flux will drop to 95% of its centre value. A value of 80% was obtained in this experiment. The difference between the two numbers may be due to the actual beam



Contours 100.0 200.0 500.0 1000. 2000.
5000. 0.1000E+05 0.1500E+05 0.2000E+05

Map of Region 2.65° North of 3C295

Figure 4.7

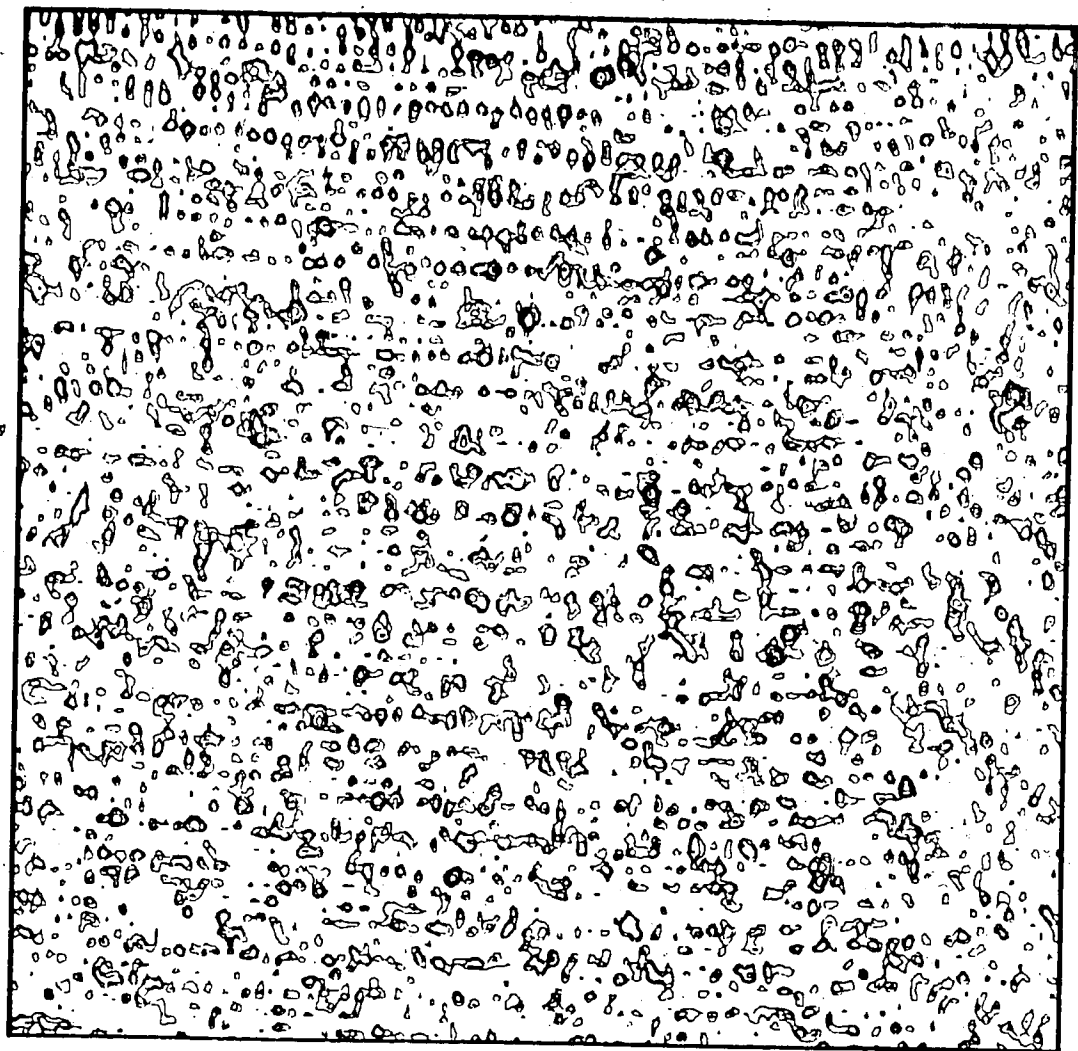
shape, the actual bandpass shape, and errors in the measurement of the half-power beamwidth.

H. Telescope Sensitivity: Maps of the 5C2 Region

The previous maps have included strong sources and the map sensitivities were limited by the dynamic range of the map rather than the noise temperature of the receiver. Thus it was desirable to observe part of the sky where there are no bright sources in order to push the instrument to its sensitivity limit.

The region mapped is called the 5C2 region and was originally mapped at 408 MHz with the Cambridge One-Mile Telescope (Pooley and Kenderdine 1968). Two nights were used to map the region in this test and the CLEANed map is shown in Fig. 4.8. The source positions and fluxes were compared with the original Cambridge survey and with later surveys (Gillespie 1979, Pauliny-Toth et al. 1972, Brundage et al. 1971, Maslowski 1971, Katgert 1975). The numbers by the sources are the 5C2 survey number, OM and OL prefixes designate Ohio Survey identifications, and other numbers refer to other surveys. 48 sources have been identified in this map.

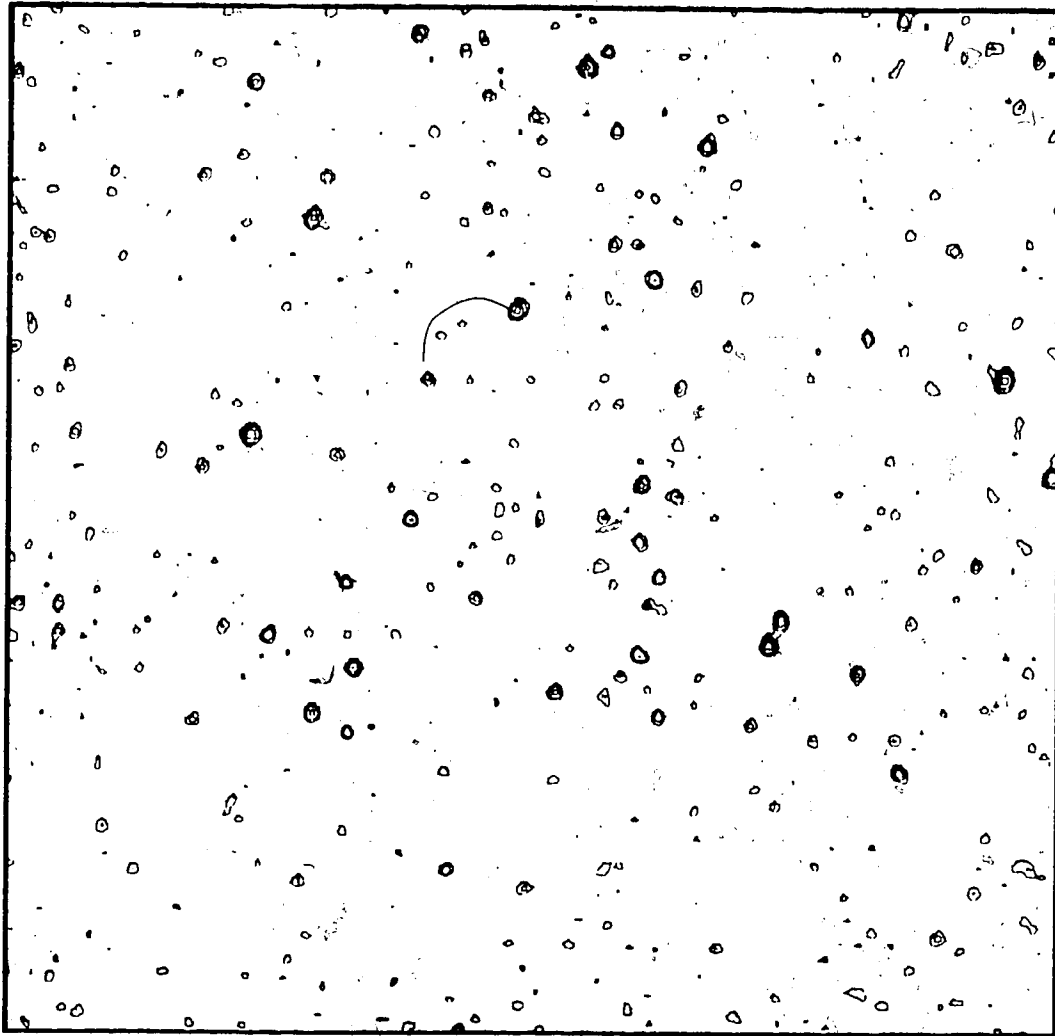
There are a number of flaws in this map. The first indication of this is that the noise level in the map is at least a factor of three too high. Thus the number of sources identified is too low. When the



Contours 250.0 500.0 1000. 2000. 4000.

CLEANed 5C2 Map with Residuals Added

Figure 4.9



Contours 250.0 500.0 1000. 2000. 4000.

Second 5C2 Map with Residuals

Figure 4.10

residuals from the CLEAN process are added back to the map (as was done with Figs. 4.6 and 4.7), Fig. 4.9 is obtained. The residuals are very large, peaking between 500 and 1000 units, and have a "striped" appearance. As shown by Thompson (1982), artifacts of this type are due to interference. With this telescope, the most probable interference signal is the spurious signal at the centre of the IF band.

A set of simple L-C notch filters were constructed and placed in the signal lines preceding the correlator. The filters have notch depths between 11 dB and 16 dB with half-power bandwidths of 120 kHz. The reduction in sensitivity due to the filters is about 1%. The 5C2 region was observed again, but for only one night, and the CLEANed map with residuals added is shown in Fig. 4.10. Stripes are not present in these residuals. This map is plotted at the same scale as the previous map. The residual peaks and standard deviation are a factor of 3.4 larger in the old map than the new map.

Before the measured map noise levels can be compared with the theoretical noise levels, the map flux scale must be calibrated. In the map making process, the calibration coefficients were selected to give a map scale of 10 units/millijansky (mJy). However, comparison of source intensities in the first map (Fig. 4.9) with well-known fluxes in previous surveys has given a ratio of 6.8 units/mJy. The source of this error is not known for certain, but it may be due to errors

introduced by the large residuals.

For a two-night map, the theoretical rms noise level is 11 mJy, and for one night it is 16 mJy. Using a conversion factor of 10 map units/mJy (6.8 units/mJy) the rms noise in the first 5C2 map is 37 mJy (54 mJy) and 11 mJy (16 mJy) in the second map. Thus it can be concluded that the notch filter has reduced the noise level in the map to approximately its theoretical level.

One further comment should be made about these maps: they were made for engineering purposes and have little astronomical value. This is because the total observing time was short and hence the amount of independent data available to make the map is small. This is especially true with the one-night 5C2 observation where a small number of data points must define a large number of sources. Thus it is not surprising to find that some real sources in the first 5C2 map are not present in the second map. However, this was a very useful engineering test to determine the suppression of the self-interference.

I. A Complete Survey: HB3 Supernova Remnant

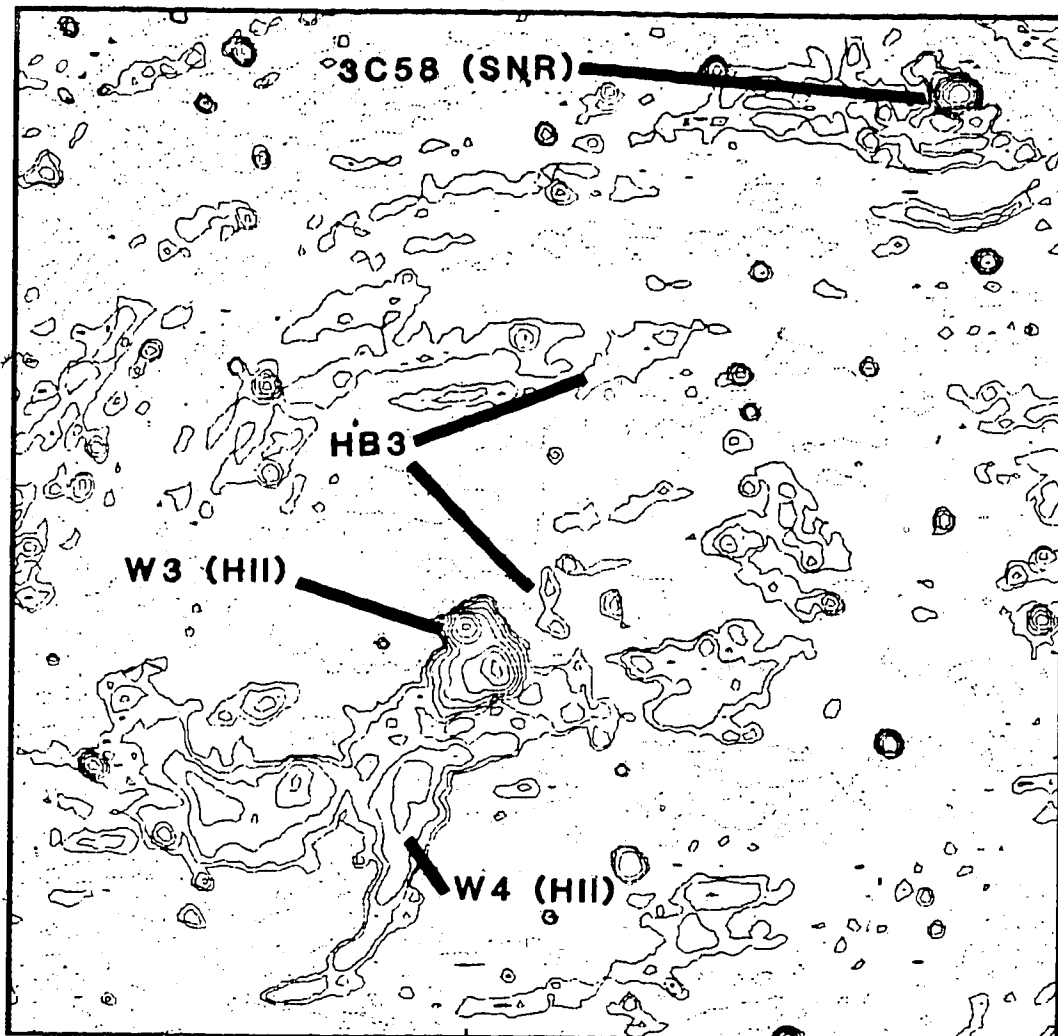
The first complete survey made at 408 MHz was of the supernova remnant HB3 and environs. HB3 subtends 70 arcminutes and the 408 MHz field also includes the HII regions W3 and W4 as well as another supernova remnant called 3C58. Maps at 38 MHz (45 arcminute beam) and

178 MHz (21 arcminute beam) were described by Caswell (1967). It has also been mapped at 2700 MHz with a 5 arcminute beam by Velusamy and Kundu (1974) and with a 12 arcminute beam by Wendker and Altenhoff (1977) and at 1420 MHz with a 9 arcminute beam (Kallas and Reich 1980). The complete shell has been observed optically by Fesen and Gull (1983) and X-ray emissions have been detected by Galas, Tuohy and Garvine (1980) using the HEAO 1 satellite. From these observations it is clear that the object is a supernova remnant because of its shell-like appearance with a central depression and its non-thermal spectral index with $\alpha = -0.52$.

These earlier observations have prompted a number of questions. HB3 lies to the north west of a "chain" of HII regions composed of W3, W4, and W5. It is not yet certain if HB3 is at the same distance as the HII regions. If it is, the expanding shock front from the supernova may be interacting with W3. In any case, the true extent of the supernova remnant has not been established because the edge of the shell is along the same line of sight as the edge of W3. Read (1981) has made HI emission maps of the region around W3 and has evidence that the neutral hydrogen is being swept up by the expanding shell.

The observations at 408 MHz are part of an attempt to answer some of these questions. The set of maps at the two frequencies can help to separate the non-thermal emission of HB3 from the thermal emission of the HII region beside it. Only preliminary results will be shown here.

Detailed analysis and interpretation are beyond the scope of this thesis. Figures 4.11 and 4.12 present the results of the HB3 survey. These maps are superior to the previous surveys in a number of ways. Most of the earlier maps suffered from poor dynamic range, which can be inferred from the fact that they displayed only 3 or 4 contour levels. The other main deficiency in the earlier maps is poor resolution; the resolution in these new maps is a factor of three better than previous maps.

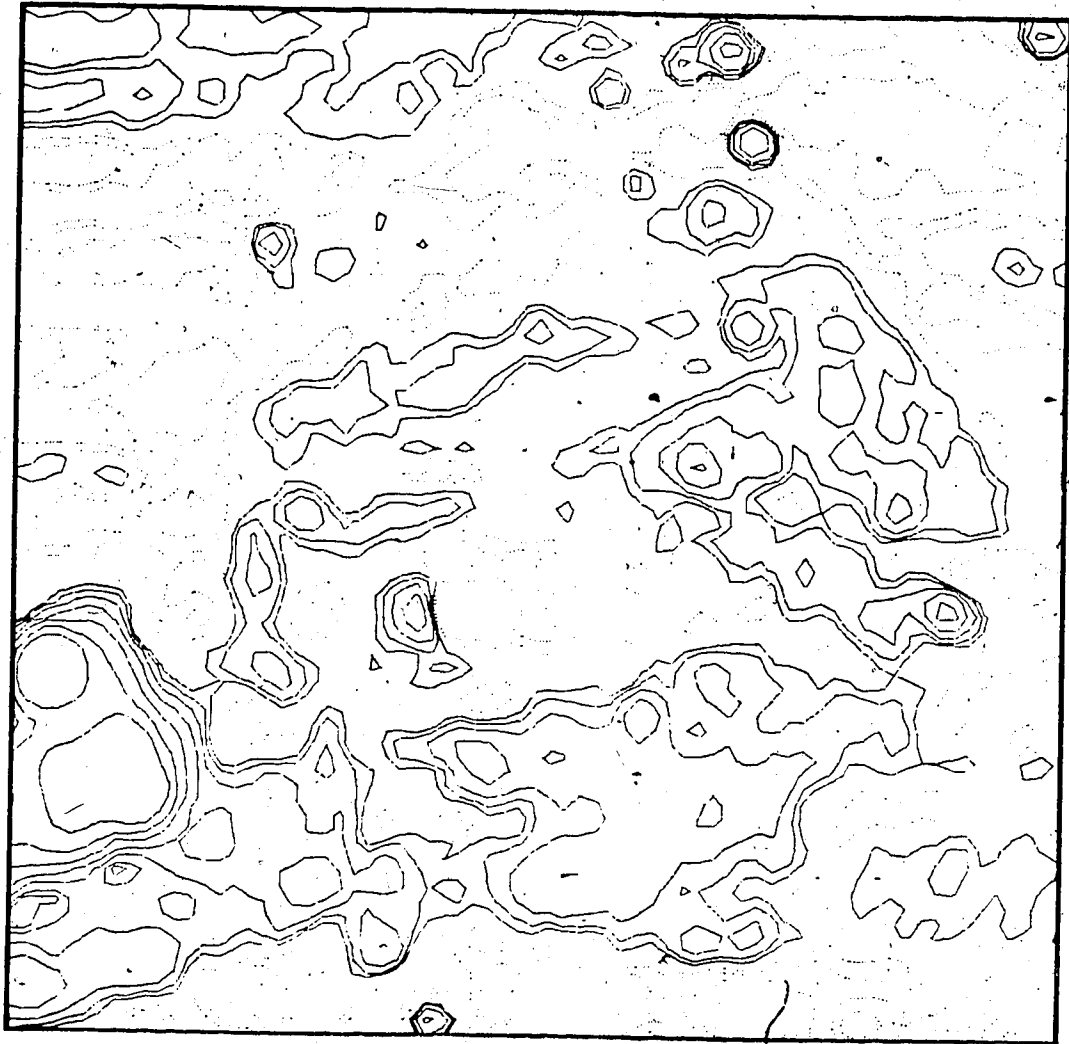


Contours	<u>-2.001</u>	<u>2.001</u>	<u>4.001</u>	<u>8.001</u>	<u>16.00</u>
	<u>32.00</u>	<u>64.00</u>	<u>128.0</u>	<u>256.0</u>	<u>x 10⁻²</u>

408 MHz Map of HB3 and Environs

(5X5 degrees)

Figure 4.11



Contours	-4.001	-2.001	-1.001	1.001	2.001
4.001	8.001	16.00	32.00	64.00	$\times 10 \text{ m}^2/\text{t} = \text{in}$

408 MHz Map of HB3 SNR (2X2 degrees)

Figure 4.12

References

- Anastassiou, A., Strutt, M.J.O., 1974, "Effect of Source Load Inductance on the Noise Figure of a GaAs FET", Proc. IEEE 62 p406
- Archer, J.W., 1977, "A Precision Phase-Controlled Local Oscillator System for a Millimetre-Wave Interferometer", IREE 16th International Radio & Electronics Engineering Convention Digest, Melbourne Aug. 8-12 pp100-102
- ARRL, 1974, The ARRL Antenna Book, American Radio Relay League, Newington, Conn.
- Baars, J.W.M., Genzel, R., Pauliny-Toth, I.I.K., Witzel, A., 1977, "The Absolute Spectrum of Cas A; An Accurate Flux Density Scale and a Set of Secondary Calibrators," Astronomy & Astrophysics 61, p99
- Baldwin, J.E., Warner, P.J., 1979, "Fundamental Aspects of Aperture Synthesis with Limited or no Phase Information," Image Formation from Coherence Functions in Astronomy, C. van Schooneveld (ed.), Reidel, Dordrecht, p67
- Blythe, J.H., 1957, "A New Type of Pencil Beam Aerial for Radio Astronomy", Mon. Not. R. Astr. Soc., 117 p644
- Bracewell, R., 1965, The Fourier Transform and Its Applications, McGraw-Hill, Toronto
- Brundage, R.K., Dixon, R.S., Ehman, J.R., Kraus, J.D., 1971, "The Ohio Survey Between Declinations of 40° and 63° North", Astronomical Journal 76 p777
- Carpenter, D.D., 1973, "The Effects of Time Delays on the Stability of Practical Phase Locked Receivers with Multiple Conversion by Utilizing Root Locus with Positive Feedback", 1973 IEEE Int. Conf. on Commun., 11, pp33-14 - 33-19
- Casse, J.L., Muller, C.A., 1974, "The Synthesis Radio Telescope at Westerbork. The 21cm Continuum Receiver System", Astronomy & Astrophysics 31 p333
- Caswell, J.L., 1967, "Radio Observations of Two Supernova Remnants", Mon. Not. R. Astr. Soc. 136 p11
- Cooke, H.F., 1982, Introduction to Microwave FETs, Varian Associates Santa Clara, CA

- deBruyn, A.G., van der Hulst, J.M., 1983, "327 MHz: Status Report and Future Outlook", Netherlands Foundation for Radio Astronomy Note 398, June 1
- Dewdney, P.E., Roger, R.S., 1982, "The HI Cloud Surrounding the Emission-Like Star LkHa 101 in the Region of NGC 1579", *Astrophysical Journal* 255 p564
- Dragone, C., Hogg, D.C., 1963, "Wide-Angle Radiation due to Rough Phase Fronts", *Bell System Technical Journal* 42 p2285
- Fesen, R.A., Gull, T.R., 1983, "The Optical Emission from the Supernova Remnant HB3", *Pub. Astr. Soc. Pacific* 95 p196
- Fomalont, E.B., 1973, "Earth-Rotation Aperture Synthesis", *Proc. IEEE* 61 p1211
- Fomalont, E.B., Wright, M.C.H., 1974, "Interferometry and Aperture Synthesis", *Galactic and Extra-Galactic Radio Astronomy*, Verschuur, G.L., Kellermann, K.I. (eds.), Springer-Verlag, New York, p256
- Forward, R.L., Cisco, T.C., 1983, "Electronically Cold Microwave Artificial Resistors", *IEEE Trans. Microwave Theory Techniques* MTT-31 p45
- Frater, R.H., Williams, D.R., 1981, "An Active 'Cold' Noise Source", *IEEE Trans. Microwave Theory Techniques* MTT-29 p344
- Galas, C.M.F., Tuohy, I.R., Garmire, G.P., 1980, "Soft X-Ray Observations of the Supernova Remnants HB3 and 3C58", *Astrophysical Journal* 236 pL13
- Gardner, F., 1974, *Phaselock Techniques*, Wiley, Toronto
- Gillespie, A.R., 1979, "Observations of the 5C1-5 Survey Areas at 1421 MHz", *Mon. Not. R. Astr. Soc.* 188 p481
- Goodman, J.W., 1968, *Introduction to Fourier Optics*, McGraw-Hill, Toronto
- Hacker, P.S., Schrank, H.E., 1982, "Range Distance Requirements for Measuring Low and Ultralow Sidelobe Antenna Patterns", *IEEE Trans. Antennas Propagation* AP-30 p956
- Haslam, C.G.T., Klein, U., Salter, C.J., Stoffel, H., Wilson, W.E., Cleary, M.N., Cooke, D.J., Thomasson, P., 1981, "A 408 MHz All-sky Continuum Survey I. Observations at Southern Declinations and for the North Polar Region", *Astronomy & Astrophysics* 100 p209

- Haslam, C.G.T., Salter, C.J., Stoffel, H., Wilson, W.E., 1982, "A 408 MHz All-sky Continuum Survey. II. The Atlas of Contour Maps", *Astronomy & Astrophysics Sup.* 47 pp1-143
- Heney, L.G., Keenan, P.C., 1940, "Interstellar Radiation from Free Electrons and Hydrogen Atoms", *Astrophysical Journal* 91 p625
- Hertz, D., Jury, E.I., Zeheb, E., 1984, "Simplified Analytical Stability Test for Systems with Commensurate Time Delays", *IEE Proc.* 131 Part D p52
- Högbom, J.A., 1974, "Aperture Synthesis with Non-Regular Distribution of Interferometer Baselines", *Astronomy & Astrophysics Sup.* 15 p417
- ITU, 1982, *Radio Regulations*, International Telecommunications Union, Geneva
- Jansky, K.G., 1933, "Electrical Disturbances Apparently of Extraterrestrial Origin", *Proc. IRE* 21 p1387
- Kallas, E., Reich, W., 1980, "A 21cm Radio Continuum Survey of the Galactic Plane Between $\ell=93^\circ$ and $\ell=162^\circ$ ", *Astronomy & Astrophysics Sup.* 42 p227
- Katgert, P., 1975, "A Third 1415 MHz Survey with the Westerbork Synthesis Radio Telescope: the 5C2 Region (Part I)", *Astronomy & Astrophysics* 38 p87
- Kiepenheuer, K.O., 1950, "Cosmic Rays as the Source of General Galactic Radio Emission", *Physical Review* 79 p738
- Koch, G.F., 1973, "Coaxial Feeds for High Aperture Efficiency and Low Spillover of Paraboloidal Reflector Antennas", *IEEE Trans. Antennas Propagation* AP-21 p164
- LaGrone, A.H., Roberts, G.F., 1966, "Minor Lob Suppression in a Rectangular Horn Antennas Through the Utilization of a High Impedance Choke Flange", *IEEE Trans. Antennas Propagation* AP-14 p102
- Landecker, T.L., 1980, *A Proposal for a Low Frequency Continuum Channel for the Synthesis Telescope*, Dominion Radio Astrophysical Observatory, Penticton, B.C.
- Landecker, T.L., Pineault, S., Routledge, D., Vaneldik, J.F., 1982, "VRO 42.05.01 - One Supernova Remnant or Two?", *Astrophysical Journal* 261 pL41
- Landecker, T.L., Vaneldik, J.F., 1982, "A Phase-stabilized Local-oscillator System for a Synthesis Radio Telescope", *IEEE Trans. Instrumentation Measurement* IM-31 p185

- Little, A.G., 1969, "A Phase-measuring Scheme for a Large Radiotelescope", IEEE Trans. Antennas Propagation AP-17 p547
- Little, A.G., Hunstead, R.W., Calhoun, G.G., 1966, "A Constant Phase Local Oscillator System for a Cross Type Radio Telescope", IEEE Trans. Antennas Propagation AP-14 p645
- Lo, W.F., 1982, A Digital Signal Processor for a 408 MHz Supersynthesis Telescope, M.Sc. Thesis, University of Alberta, Edmonton
- Maslowski, J., 1972, "A Green Bank Sky Survey in Search of Radio Sources at 1400 MHz. II. Spectral Properties of the 5C1 and 5C2 Sources", Astronomy & Astrophysics 16 p197
- Millman, J., Halkias, C.C., 1972, Integrated Electronics: Analog and Digital Circuits and Systems, McGraw-Hill, Toronto
- Minnett, H.C., Thomas, B.M., 1968, "Fields in the Image Space of Symmetrical Focusing Reflectors", Proc. IEE 115 p1419
- Napier, P., 1982, "VLA 327 MHz Prototype Feed System", VLA Electronics Memorandum #206, NRAO, Socorro, N.M.
- Napier, P.J., Crane, P.C., 1982, "Signal-to-Noise Ratios", Lecture #3, Synthesis Mapping, Proc. NRAO-VLA Workshop, Socorro, NM, June 21-25, Thompson, A.R., D'Addario, L.R. (eds.) National Radio Astronomy Observatory, Green Bank, W.V.
- Napier, P.J., Thompson, A.R., Exers, R.D., 1983, "The Very large Array: Design and Performance of a Modern Synthesis Radio Telescope", Proc. IEEE 71 p1295
- NRAO, 1967, A Proposal for a Very Large Array Radio Telescope, National Radio Astronomy Observatory, Green Bank, W.V.
- Ogata, K., 1970, Modern Control Engineering, Prentice-Hall, Englewood Cliffs, N.J.
- Oort, J.H., Kerr, F.T., Westerhout, G., 1958, "The Galactic System as a Spiral Nebula", Mon. Not. R. Astr. Soc. 118, p379
- Pauliny-Toth, I.I.K., Shakeshaft, J.R., 1962, "A Survey of the Background Radiation at a Frequency of 404 Mc/s", Mon. Not. R. Astr. Soc. 124 p61
- Pauliny-Toth, I.I.K., Kellerman, K.I., Davis, M.M., Fomalont, E.B., Shaffer, D.B., 1972, "The NRAO 5-GHz Radio Source Survey. II. The 1420-Ft. 'Strong', 'Intermediate', and 'Deep' Source Surveys", Astronomical Journal, 77 p265

- Percival, W.S., 1939, "An Electrically 'Cold' Resistance", *Wireless Engineer*, May 1939, p237
- Pooley, G.G., Kenderdine, S., 1968, "The 5C2 Survey of Radio Sources", *Mon. Not. R. Astr. Soc.* 139 p529
- Purton, C.R., 1983, Proposal for Observations with the Synthesis Telescope, Dominion Radio Astrophysical Observatory, Penticton, B.C.
- Rahmat-Samii, Y., 1983, "An Efficient Computational Method for Characterizing the Effects of Random Surface Errors on the Average Power Pattern of Reflectors", *IEEE Trans. Antennas Propagation* AP-31 p92
- Read, P.L., "HI Aperture Synthesis Observations Towards Galactic HII Regions - II. W3", *Mon. Not. R. Astr. Soc.* 194 p863
- Reber, G., 1940, "Cosmic Static", *Proc. IEEE* 28 p68
- Reber, G., 1944, "Cosmic Static", *Astrophysical Journal*, 100 p279
- Roger, R.S., Costain, C.H., Lacey, J.D., Landecker, T.L., Bowers, F.K., 1973, "A Supersynthesis Radio Telescope for Neutral Hydrogen Spectroscopy at the Dominion Radio Astrophysical Observatory", *Proc. IEEE* 61 p1270
- Ryle, M., 1962, "The New Cambridge Radio Telescope", *Nature* 194 p517
- Saleh, A.A.H., 1981, "Planar Multiport Quadrature-like Power Dividers/Combiners", *IEEE Trans. Microwave Theory Techniques* MTT-29 p332
- Scheffer, H., 1975, "Improvements in the Development of Coaxial Feeds for Paraboloidal Reflector Antennas", Paper B1/2, 5th European Microwave Conference, Hamburg
- Shimozawa, D.T., 1968, Coherent Local Oscillators for a 21 cm Supersynthesis Experiment, MASC Thesis, University of British Columbia, Vancouver
- Silver, S., 1949, *Microwave Antenna Theory and Design*, McGraw-Hill, Toronto
- Steer, D.G., 1984, "A Study of Image Recovery Techniques for Radio Long Baseline Interferometry", Ph.D. Thesis, University of British Columbia, Vancouver

- Stute, U., Reich, W., Kalberla, P.M.W., 1980, "High Dynamic Range Observations in the Fields of Strong Extragalactic Radio Sources", *Astronomy & Astrophysics Sup.* 42 p299
- Swarup, G., Yang, K.S., 1961, "Phase Adjustment of Large Antennas", *IRE Trans. Antennas Propagation* AP-9 p75
- Thompson, A.R., 1981, "Directional Frequency Offsets in Round-trip Phase-measuring Schemes, With Application to the IRAM Array and the VLA", VLA Electronics Memo #202, National Radio Astronomy Observatory, Socorro, N.M.
- Thompson, A.R., D'Addario, L.A., 1982, "Frequency Response of a Synthesis Array: Performance Limitations and Design Tolerances", *Radio Science* 17 p357
- Thompson, A.R., 1982, "The Effects of Bandwidth and Similar Parameters", Lecture #5, Synthesis Mapping, Proc. NRAO-VLA Workshop, Socorro, N.M., June 21-25, Thompson, A.R., D'Addario, L.R., (eds.), National Radio Astronomy Observatory, Green Bank, W.V.
- Thompson, A.R., 1982, "The Response of a Radio-Astronomy Synthesis Array to Interfering Signals", *IEEE Trans. Antennas Propagation* AP-30 p450
- van der Hulst, H.C., 1945, "Herkomst der radiogolven uit het wereldruim", *Nederlandsch Tijdschrift voor Natuurkunde* 11 p210; or in English, *Classics in Radio Astronomy*, Sullivan, W.T. (ed.) Reidel, Dordrecht, p302
- Velusamy, T., Kundu, M.R., 1974, "Observations of Intensity and Linear Polarization in Supernova Remnants at 11cm Wavelength", *Astronomy & Astrophysics*, 32 p375
- Weinreb, S., Fenstermacher, D.L., Harris, R.W., 1982, "Ultra-low-noise 1.2-to 1.7-GHz Cooled GaAsFET Amplifiers", *IEEE Trans. Microwave Theory Techniques* MTT-30 p849
- Wendker, H.J., Altenhoff, W.J., 1977, "A 2695 MHz Map of the IC1795 1805/1848 Region", *Astronomy & Astrophysics* 54 p301

END

2 7 0 6 8 6

FIN